

Chapter 2

Circulation and Mixing in Estuaries

2.1 Hydrologic Processes: Ocean-Drainage Basin-Estuary

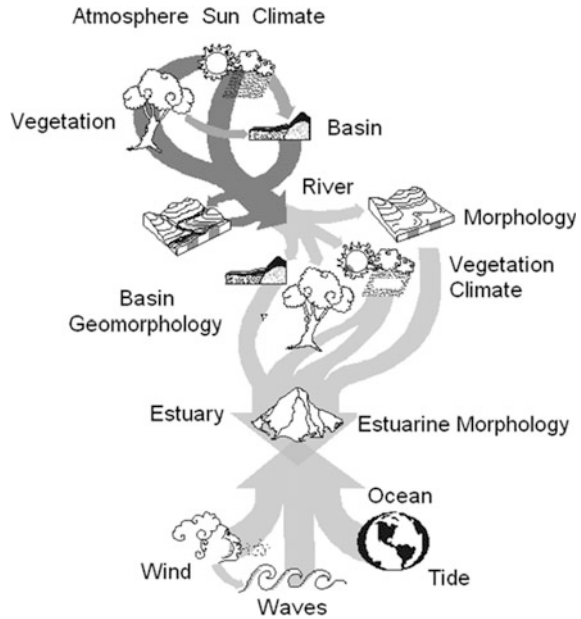
An estuary is a coastal transitional environment between the continental land masses and the ocean, where the sea water is diluted by fresh water from continental drainage basin. This environment is forced by local and remote processes generated by climatic, oceanographic, geological, hydrographic, biological and chemical events, occurring in the ocean and drainage basin at distances, as far as, thousands of kilometers away.

The drainage basin is the catchment origin of the river system, which empties into the estuary, supplying not only water but also sediments, organic and inorganic substances and eventually pollutants. The fresh water budget of a drainage basin is dependent on the climatic conditions, soil characteristics, vegetation area and uses (urban, agriculture and industrial), evaporation and transpiration from surface water, and its interactions are illustrated in Fig. 2.1, according to Coleman and Wright (1971). This fresh water budget of a hydrographic basin is only a small fraction of the global hydrologic cycle, which is defined as the movement and endless recycling of water between the atmosphere, the land surface, and the ground.

With human development and occupation of the land adjacent to estuaries occurring after the second half of the XIX century, the geometry and hydrologic conditions of the drainage basins of rivers were gradually and drastically altered. These alterations resulted from the construction of dams, water barriers and channels (such as the Valo Grande channel in the estuarine- lagoon system of Cananéia-Iguape—Fig. 1.5), forest destruction, and road and pavement construction, which interfered deeply in the natural ecological characteristics of these coastal environments.

Solar radiation is the main energy source in our planet. Its distribution on the earth's surface varies according to the geographic latitude and the seasons of the year. The cloud cover, aerosols and particle concentrations in the atmosphere, also

Fig. 2.1 Local and remote processes and forces in the catchments and in the ocean, which contributes to the estuaries characteristics and dynamics (according to Coleman and Wright 1971)



influence the solar energy reaching the earth's and ocean's surfaces. This energy flux controls the heat concentration in the oceans and atmosphere. It is the only energy source that drives the processes of evaporation and transpiration in the estuary catchment region, and primary production through the photosynthesis of microscopic organisms (phytoplankton) and zooplankton, which supports the estuaries feeding chain in the estuaries.

The wind stress forcing promotes the aeration of the estuary surface layers and the mixing of the estuarine and coastal water masses, and may erode the vertical salinity gradients, mainly in the estuary's mouth sheltered from local weather. This forcing may also generate currents, waves, intensifying the vertical mixing, mainly in estuaries with large surface area. Characteristics on the induced circulation in the Potomac river estuary (Virginia, USA), has been investigated in the paper of Elliott (1978), based on the analysis of meteorological data and current measurements at three depths. It was shown that the non-tidal currents were responding to two distinct forcing mechanisms of almost equal importance: the local and non-local wind effects propagating into the estuary from the Chesapeake Bay.

The precipitation, river discharge and evaporation-transpiration in the estuary catchment is always positive, i.e., the sum of the fresh-water source (precipitation and river discharge) is always higher than the sink (evaporation-transpiration). This is in agreement with the Pritchard (1955) definition, stating that in the estuary the seawater is measurably diluted by the fresh water discharge. The main factors that may influence this balance are the temperature and relative air humidity, the wind direction and intensity, the geomorphology of the catchment region, the soil characteristics and vegetation (Fig. 2.1).

The river discharge into the estuary gradually dilutes the sea water due to the advection and turbulent diffusion, generating the longitudinal salinity (density) gradient, which are of fundamental importance to the estuary dynamics. The river discharge (Q_f) is physically defined as a volume transport (volume per time unity). The ratio of the volume transport by any transversal section of the estuary is the intensity of the mean velocity u_f , (distance per time) across the section forced by the river discharge; these quantities have dimensions of $[Q_f] = [L^3T^{-1}]$ and $[u_f] = [LT^{-1}]$, respectively. As will be seen later, this quantity is one of the low frequency components of the estuary seaward motion, and it is the result of the application of the mass (volume) conservation equation integrated over the estuary domain.

In most nations, there are governmental entities which are responsible for monitoring the river discharges of small and large rivers. In medium and high latitude regions, the snow height accumulated during the winter time is used to forecast the availability of fresh water; as the snow melts at the end of winter and during spring, an important volume of fresh water is added to the catchment regions. In general, the fresh water discharge is monitored with measurements of the relative height of the river surface (once a day or with continuous sampling), which are converted to discharge estimates with a calibration equation of the equipment. In the rivers flowing into the sea, these measurements are made far from the estuary head or tidal river zone (TRZ), where the motion is unidirectional. These data are stored in official water and energy management institutions, and may be easily accessed.

It is desirable that the river discharge (Q_f) is considered as known data when focusing on problems related to estuarine physics, because its long term monitoring and determination is from the dominion of Hydrology. Because, in general, this physical quantity is measured for the purpose of controlling the availability of the fresh water supply for urban communities, industrial plantations and agriculture, and not specifically for estuarine research.

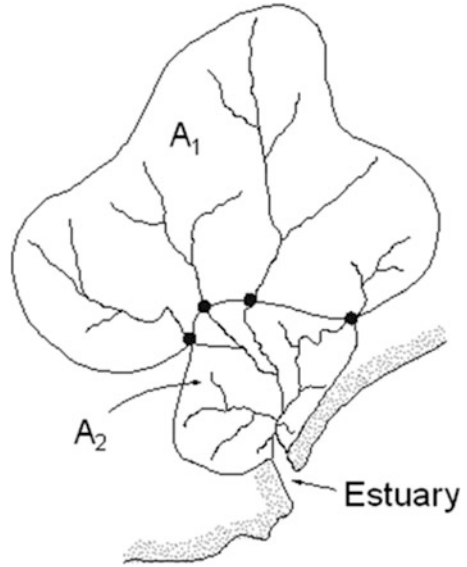
In Fig. 2.2 is presented schematically a catchment area with river discharge towards the coastal region occurring through an estuary. Let us assume that this catchment is composed of several rivers and tributaries with its discharges being measured at the monitoring stations, indicated by black circles. In this figure, A_1 is the total monitored catchment area and, let us indicate by q_i a generic river discharge of the station i (in this case $i = 1, 2, 3$ and 4). Then, the river discharge contribution (Q^*) of the monitored area (A_1) is calculated by:

$$Q^* = \sum_i q_i, \quad i = 1, \dots, 4, \quad (2.1)$$

which doesn't take into account the partial catchment area (A_2), localized seaward of the monitoring stations, thus $Q^* < Q_f$.

However, as the total river discharge to be calculated is Q_f , it is necessary for a correction to be applied to the partial discharge Q^* . In the hypothesis that the precipitation and evapo-transpiration processes have the same values in both areas

Fig. 2.2 Schematic diagram of an estuary catchment area ($A_1 + A_2$) of main rivers and its tributaries. A_1 is the partial area of the monitored rivers discharges at the stations indicated by *black dots*



and are uniform in the total area ($A_1 + A_2$) and that the soil characteristics are also the same, we may estimate a dimensionless correction (c), which is given by:

$$c = \frac{(A_1 + A_2)}{A_1}, \quad (2.2)$$

with $c \geq 1$; and $c = 1$ when $A_2 \rightarrow 0$, and the river discharge monitoring stations are located at the estuary mouth, which is not the case. Then, with these results it follows that the best value of the river discharge at the estuary head is given by:

$$Q_f = cQ^*, \quad (2.3)$$

where c is a correction factor. From this equation, it follows that if $A_1 \gg A_2$, then $c \approx 1$ and $Q^* \approx Q_f$.

The river discharge input at the estuary head occurs with a delay in relationship its measurements at the up-river gauging stations. Because gauging stations are often located further upstream and away from the estuarine zone. In turn, these measurements also have a delay in relationship to the precipitations at the catchment area, where the processes that determine the water volume of the surface flow in the river and its tributaries occur; however, in general, these time intervals are very difficult to calculate and are usually not taken into account. Besides the seasonal time scale dominance in the river discharge (Q_f), daily time variations may also occur due to the abnormal short time precipitations. Then, in order to have representative values of river discharges for a given experiment, it is advisable to use daily mean values of a time series measurements.

The problem of estimating the river discharge in an estuarine system is illustrated for the river system of the catchment area emptying into the Winyah Bay ($33^{\circ} 15'N$), localized in the South Carolina State (USA). Based on monitored river discharges from the main river and some tributaries, this estuarine system has an annual mean fresh water discharge of $557 \text{ m}^3 \text{ s}^{-1}$. The fresh water input and low contributions. Taking into account the monitored main catchment area, (A_1), and the catchment area localized seaward of the monitoring stations (A_2), Eq. (2.2) was used to calculate the correction factor c ($c = 2.1$). This factor was applied to the daily discharge values of the tributaries in the area A_1 (Eq. 2.3) in order to obtain a more representative time series of the river discharge into the Winyah Bay (Fig. 2.3). In this figure it may be observed that the $Q_f = Q_f(t)$ time series is a non-stationary quantity, presenting daily and seasonal variability. The following river discharge regimes were also found in this data analysis:

- (i) A moderate river discharge from April to June, varying from 200 to $1000 \text{ m}^3 \text{ s}^{-1}$;
- (ii) In the transitional period from June to July, a secondary maximum of $1600 \text{ m}^3 \text{ s}^{-1}$ occurred, which decreased in a few days to reach the lowest values between August and November ($200 \text{ m}^3 \text{ s}^{-1}$);
- (iii) As the result of the ice melting at the end of the winter season, the highest river discharges occurred during February ($Q_f > 4000 \text{ m}^3 \text{ s}^{-1}$).

River discharges have been monitored for many rivers around the world from the early 1900s. In Brazil, the National Electricity Agency (ANEEL), through the National Water Agency (NWA), is responsible for discharges and water quality measurements, for most Brazilian states, with exception of the São Paulo state, whose river discharge measurements are made by the Department of Water and Electrical Energy (DAEE). In the Jaguaribe river in NE Brazil (Ceará), for example,

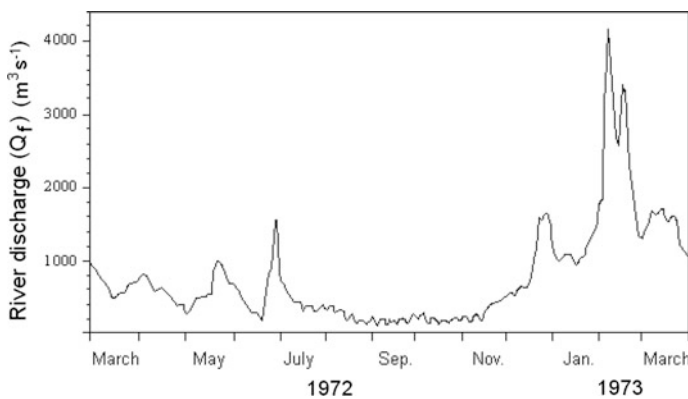


Fig. 2.3 Temporal variability of the river discharge into Winyah Bay (South Caroline, USA). Q_f was estimated by the sum of the daily discharges in the catchments of the main tributaries, extrapolated to the estuary head with the application of the correction factor (Eq. 2.2)

there are 11 pluviometric stations with 80 years of monitoring, plus 11 river discharges monitoring stations, performing 25 years of continuous data (Lacerda et al. 2002), and the Itajai-açu river (Santa Catarina) has been monitored since 1934 (Schettini 2002). However, it should be noted that major rivers affecting the coastal zone may have caused environmental problems due to river diversion, damming, and industrial effluent releases, which affect the river discharge, addition to eutrophication, pathogen contamination, toxic chemicals, loss of habitat, and declines in fish and wildlife.

For estuary catchment areas, or any coastal environment (bay, inlet, coastal lagoon) where rivers discharges have not been monitored, this quantity may be indirectly estimated using semi-empirical methods. First of all, let's introduce the definition of *surface runoff tax*, Δf , as the precipitation rate (P) generating a runoff which discharges into the river; both Δf and P are expressed as height per time [LT^{-1}]. The ratio of these quantities defines the dimensionless *surface runoff ratio* ($\Delta f/P$) as a dimensionless quantity, which must depend on the rainfall itself; when rainfall is so heavy that evaporation can only remove a small fraction of the annual water accumulation in the catchment area, the runoff ratio must approach unity ($\Delta f/P \rightarrow 1$). Conversely, in extreme cases when rainfall is so sparse that evaporation can easily remove the annual water accumulation, the runoff ratio approaches zero ($\Delta f/P \rightarrow 0$).

The maximum annual evaporation is, of course, strongly dependent on the intensity of solar radiation. Various functions have been proposed that relate the runoff ratio ($\Delta f/P$) to the rainfall, P . The simplest of these functions was introduced by the German hydrologist P. Schreiber, in 1904 (quoted in Holland 1978), who found that the runoff ratio for central European rivers was related to the rainfall (P) by the expression, already adapted for the effect of latitude on the runoff ratio (Holland, op.cit.):

$$\frac{\Delta f}{P} = \exp\left(-\frac{E_v}{P}\right), \quad (2.4)$$

which states the relationship of the surface runoff ratio and the exponential ratio of E_v/P (the annual mean potential evapotranspiration rate and the corresponding precipitation).

The dependence of the first term in Eq. (2.4), on the evaporation rainfall tax, has already been discussed, and is in agreement with this equation because it decreases exponentially between the extreme values 0 and 1 when $E_v \gg P$ and $E_v \ll P$, respectively, and represents the rainfall tax which will effectively take part in the surface runoff.

Schreiber's equation (2.4) predicts that the runoff ratio should be latitude dependent, because the evaporation decreases rapidly due to the low temperatures at high latitudes, which has been confirmed by Kosoun et al. (1974). Thus, the exponential decrease of E_v with increasing latitude between the extreme values 0 and 1, for $E_v \gg P$ and $E_v \ll P$, respectively, confirms the physical basis of the Schreiber's equation.

The evapo-transpiration potential (E_v) has an accentuated decrease with temperature towards high latitudes. The runoff ratio's ($\Delta f/P$) dependence on latitude was experimentally obtained with data of representative catchments of Europe, Asia, Africa, Australia and North and South America, including the Amazon and São Francisco rivers. Although this dependence indicates a greater scatter at low latitudes, it was possible to confirm the physical basis of the P. Schreiber equation (Eq. 2.4) and to establish, with curve fitting procedure, the following equation for determining E_v as function of the annual mean absolute surface air temperature (T), according to Holland (1978):

$$E_v = 1.2 \times 10^9 \exp\left(-\frac{4.62 \times 10^3}{T}\right). \quad (2.5)$$

In this equation the temperature is expressed as K, and E_v , $[E_v] = [LT^{-1}]$ is calculated in cm year^{-1} , with satisfactory can be applied in the range from the Equator to about 70° of latitude (north and south), and thus excluding high latitude areas. This method only gives representative values when calculated using monthly or annual mean temperature and precipitation values for long time periods (Kjerfve 1990).

Thus, to estimate the runoff ratio ($\Delta f/P$), it is necessary to know the mean values of the surface air temperature (T), the rainfall tax (P), the catchment area (A_T), and the time interval (Δt) used to calculate the mean values of E_v and P . Then, the river discharge may be obtained with the following equation:

$$Q_f = \frac{\Delta f}{P} (PA_T) = \Delta f A_T. \quad (2.6)$$

We can observe in this equation that the river discharge, calculated by the product of the precipitation tax by the catchment area (PA_T), is corrected by the runoff ratio ($\Delta f/P$). The result this equation to calculate the river discharge Q_f is in unities of $\text{cm}^3 \text{ year}^{-1}$, according to the units indicated above. However, using a convenient conversion factor, it is possible to calculate the river discharge in the International System of Units ($\text{m}^3 \text{ s}^{-1}$).

In order to exemplify this method, the following data of the catchment area and meteorological data of the Santee river (South Caroline, USA) is used: $A_T = 41 \times 10^3 \text{ km}^2 = 41 \times 10^9 \text{ m}^2$, $T = 20^\circ\text{C} = 293 \text{ K}$ and $P = 1.25 \text{ m year}^{-1}$. Applying Eqs. (2.5) and (2.6), it follows: $E_v = 170 \text{ cm ano}^{-1}$ and $\Delta f/P = 0.25$, and in Eq. (2.6) the final result is: $Q_f = 1.28 \times 10^{10} \text{ m}^3 \text{ ano}^{-1} \approx 406 \text{ m}^3 \text{ s}^{-1}$; this value is about 25% lower than the mean river discharge based on river measurements previously indicated ($557 \text{ m}^3 \text{ s}^{-1}$).

As already indicated, the factor 1.2×10^9 of the exponential function in Eq. (2.5) was adjusted for the runoff ratio $\Delta f/P$ to be calculated with Eq. (2.4) in units of $\text{cm}^3 \text{ year}^{-1}$. However, with monthly mean values of a long time series of air temperature, it is possible to obtain the monthly and the seasonal variation of the river discharge in an estuary (or in any other coastal environment). In this case, it is

easily to show that to calculate E_v in mm monthly^{-1} , the factor must be altered to 1.0×10^9 .

This method has been applied by Medeiros and Kjerfve (1993) to calculate the seasonal variation of the river discharge into the tropical estuarine system of the Itamaracá (Pernambuco, Brazil—07° 50'S; 034° 50'W) during the peak rainy ($57.7 \text{ m}^3 \text{ s}^{-1}$) and dry seasons ($0.2 \text{ m}^3 \text{ s}^{-1}$). With these results, it was possible to conclude that the freshwater input variation dominates the system behavior. During the rainy season the system is partially mixed, and gravitational circulation prevails; however, in the dry season the estuary becomes well-mixed due to the low freshwater discharge. Normalized data of air temperature and precipitation time series of several years, from meteorological stations representative to the Saquarema and Araruama coastal lagoons, Guanabara bay (Rio de Janeiro, Brazil) and for the estuarine-lagoon system of Cananéia-Iguape (Fig. 1.5), were also used to estimate the freshwater discharges in these systems (Schettini 1994; Kjerfve et al. 1996, 1997; and Bonetti and Miranda 1997).

When the catchment area extends over large areas, the results of the fresh water discharge will be more representative, if mean data values of air temperature and rainfall in the subareas of the catchment are known, enabling calculation of partial results. Applying the procedure presented above, the sum of these partial results will be the total freshwater discharge into the system.

Equilibrium conditions between the freshwater input in the estuary head and the outflow to the adjacent coastal region remains, in general, under nearly steady-state conditions. In this condition, the resulting time mean volume transport during several tidal cycles, across transversal sections located in the estuary head and mouth, will have almost the same value. The evaporation, precipitation, spring water and percolation at the bottom processes, usually have a small contribution to the freshwater balance in the estuarine system.

Besides the secular influence of the air temperature over the hydrologic cycle in the last one hundred years, abnormal events of dry weather and flooding related to the anomalies of the sea surface temperature (SST) have also occurred, with intervals varying from one to seven years.

The more catastrophic dry climate that remained for 83 days occurred in the USA in 1986. This was correlated with high sea surface temperatures ($>32^\circ \text{C}$) in the North Atlantic, whose influence on the hydrologic cycle caused a reduction by almost 50% on the rivers discharges. Besides the social and economic problem, this dry climate also produced an increase in the salinity of the estuarine water masses with the following consequences to the biological community:

- Great mortality of fishes and crustacean community.
- Reduction of larvae recruitment.
- Turbidity increase in the water mass during the recovery of the normal hydrologic cycle, with great impact on biological and algae production.

The SST increase also creates favorable conditions to the occurrence of violent storms and hurricanes in tropical and subtropical regions. These transient events,

reaching coastal environments, are usually strong enough to produce impacts with alterations in the sea level, coastal and estuarine circulation, biological, chemical and erosive processes. Then, we may propose the following questions of fundamental ecological importance:

- What will be the biological and physical alterations in the estuaries, due to the climatic transient changes, and due to long time periods (decades, centuries and millennia)?
- When will there be an occurrence of changes in the coastal region?
- How to grant and maintain the sustainability of the estuary development due to the natural and human alterations?

2.2 Temporal and Spatial Scales of Sea-Level Variations

The formation history and localization of estuaries were dependent on the secular variations of the relative sea level which occurred during the Holocene sea level transgression (Fig. 1.1, Chap. 1). After reaching the current sea level, its variation on time scales of seconds (wind waves), hours (astronomic tidal waves), days (waves generated by meteorological forcing), months (vortices and meanders of oceanic currents), annual (seasonal variations in the ocean-atmosphere processes and steric level variations), inter-annual and decadal (climatic interactions generated by global processes as El Niño), started to exert influences with different intensities on the hydrodynamic behavior of estuaries.

The time scales, characterizing the estuarine variability can be described as being either *intratidal* or *subtidal* (Jay 2010):

- (a) Intratidal—variability which occurs at semidiurnal or diurnal tidal frequencies >1 cycle/day (periods of 12–25 h), or shorter time periods (Fig. 2.4a, b), and their *overtides* driven by non-linear processes occurring at sums or multiples of the basic astronomical frequencies, are the most obvious examples of intratidal variability. Also classified in this category are (i) the variations of scalar properties (e.g., salinity, temperature and density) driven directly by tidal currents; (ii) the effects of daily sea breeze, harbor seiches with periods of minutes to hours; (iii) internal waves; and (iv) in large estuaries inertial motion at the local pendulum frequency (periods of 12–20 h at mid-latitudes).
- (b) Subtidal—variability at frequency of <1 cycle/day. In this category are included low-frequency tidal motions as the fortnightly and monthly tidal modulation of the M_2 and S_2 tidal components—periods of 13–15 days, and M_2 and N_2 —periods of 28–30 days, and variability related with weather systems with typical periods 3–10 days (Fig. 2.4c), or even at longer time periods, such as seasonal in response to the changes in the river discharge and snow melting events (Fig. 2.4d).

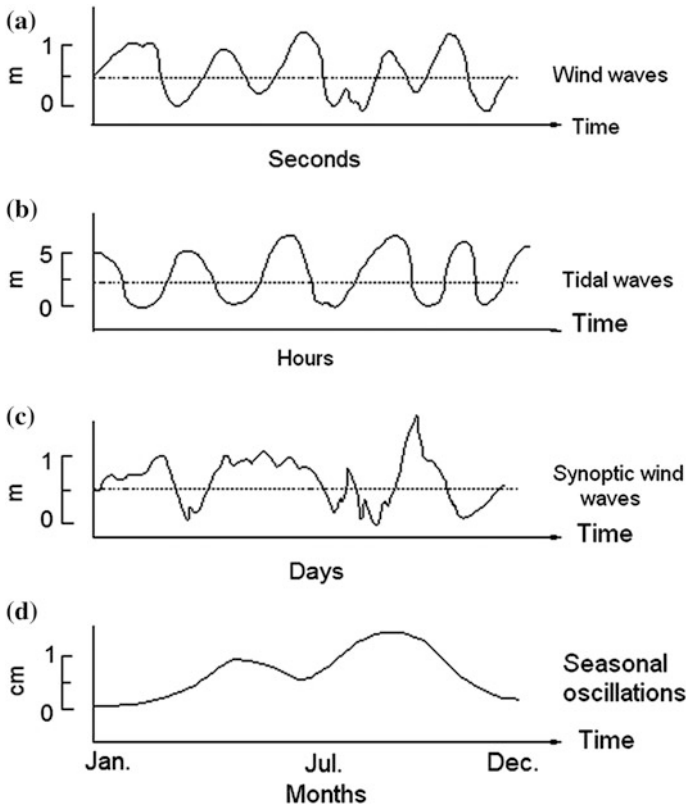


Fig. 2.4 Time and height variations of the sea level. Intratidal (a, b); wind waves (or gravity waves) and tidal waves and, subtidal (c, d); synoptic wind waves and seasonal oscillations

- (c) Motions that do not vary in time and space are classified as *steady-state* and *uniform*, respectively.

Wind waves generally have a greater influence over the mixing processes in shallow estuaries with large surface area. In some estuarine systems, this influence is more accentuated at the estuary mouth, which is the region more intensively forced by these waves remotely generated on the continental shelf and the open ocean.

The astronomic tide forcing is dominant in generating motions (turbulent and circulation, in low scale large scale, respectively), producing mixing of the fresh-water and salt water, thus evolving the processes of advection and diffusion, which vary spatially and are also influenced by the estuary geometry. In relation to this forcing, it is necessary to distinguish between the tidal oscillation and tidal co-oscillation. It is known that the tidal phenomenon is generated by the gravitational attraction of the Moon and the Sun, associated with centripetal acceleration, acting directly in the great ocean water masses. The action of this gravitational

phenomenon on the estuarine water masses is negligible. However, the global tide generation in the ocean propagates towards the continental shelf in different types of waves (Kelvin, Poincaré and gravity long waves), being one of the main generating motions and mixing processes in the estuaries; their influence propagates up and down estuary as a long wave of gravity. The tidal forcing in the estuary, which has the same period as the oceanic tide is denominated as *co-oscillation tide* (Defant 1960).

The origins of the sub-tidal fortnightly modulation are not as simple as the equilibrium tidal theory implies, and to understand them requires knowledge of both equilibrium and dynamic tidal theory, and the inter-relationships with the tidal constituents: synoptically driven neap-spring cycles occurs, when the M_2 and S_2 tidal constituents dominate the tides, and tropically driven neap-spring cycles occurs when the tidal constituents O_1 and K_1 are prevalent (Kvale 2006). In this low frequency band there is also a distinctive separation between its spectral characteristics. With periods of days and weeks we may observe the random occurrence of continental shelf waves. These topographic waves are generated by the oscillation in the synoptic scale of the wind component parallel to the coast (Gill and Schumann 1979). Also, within this time scale the sea level may respond in phase to the wind components (mainly parallel to the coast) and to the atmospheric pressure oscillations generating wind storms. Since the sea surface responds as an inverted barometer to the atmospheric pressure, these oscillations are also able to rise up or lower the sea surface level by about one centimeter for each decrease or increase of one millibar in the atmospheric pressure, respectively.

Meanders and vortices of oceanic currents may propagate through the continental shelf, reaching the coastline. The typical temporal scale of this process is about one month, having the same signature of the up and down elevation of the sea level, considering these to be anti-cyclonic and cyclonic, respectively. However, the possibility of influence of these phenomena in the estuaries is restricted to narrow continental shelves with abrupt topography. Seasonal meteorological processes, such as the predominant wind direction or atmospheric pressure fields over the continental shelf, may also be the forcing of the annual oscillations of the sea level at the estuaries mouth.

At larger time scales, such as several years, climatic global processes such as the El-Niño-Southern Oscillation may influence the sea surface height along the coastline where its intensity may be stronger and with longer duration. The typical El-Niño influence, for example, is characterized by the upwelling interruption usually present along a great extension of the Equatorial South America west coast, mainly Peru. It is known that the upwelling occurrence is only possible when the sea level at the coastline remains lower than the mean sea level (from approximately 0.01 to 0.1 m). Thus, during the time occurrence of this global phenomenon which may last for several months the sea level in the Peru coast and, consequently, at the estuaries mouth will remain lower or higher than in normal conditions, with influences on the physical and ecological characteristics of these transitional water bodies.

However, although this large temporal time scale of the sea level oscillation and with simultaneous high frequency oscillations, the hydrodynamics characteristics of

estuaries are mainly controlled by the semi-diurnal and diurnal tidal oscillations. The differences in magnitude and duration between ebb and flood currents, produced by the distortion of the tide wave propagating on the costal shelf and entering bays and estuaries, are named *tidal asymmetry*.

The oceanic tide was one of the first oceanographic phenomena theoretically studied. Using Newtonian concepts of Mechanics, the equilibrium tidal theory was developed in the pioneering scientific work of Daniel Bernoulli, in 1740. The main components of the tidal oscillation were calculated by P.S. Laplace, in 1775. In subsequent work, the tide effect was subdivided into oceanic and shallow water tides, with contributions from several notable researchers, for example, those mentioned in the von Arx (1962) book. However, even with the work of these researchers and attempts to find the tidal heights in real time using the solutions of the Laplace equations, the problem of how to compute the theoretical tide forecast from its basic principles remained to be solved. The prevision of tidal heights needs experimental data from sea level height measurements in coastal and open ocean tidal stations.

Over the continental shelf, the tide wave is transported by a complex set of waves influenced by the Earth's rotation. This transport is highly dependent on the width and bottom topography on the continental shelf. In continental shelves with wide width (order of 10^5 m), the tide co-oscillates with the adjacent deep ocean, which may present amplifications during its propagation from the continental shelf break up to the coastline. Poincaré waves predominate in the energy transport across the continental shelf. However, in narrow continental shelves the tidal wave is usually a propagate wave; along the coastline it propagates as Kelvin and Poincaré waves. In general, however, the tidal wave propagation on the continental shelf is a combination of co-oscillation and propagation and the influence of these characteristics on estuarine processes are not well understood. Upon entering an estuary, the water depth becomes shallow and the tidal wave is observed to become more asymmetric as it travels upstream. The explanation for this increasing asymmetry lies in the fact that friction causes the wave to travel at a speed (celerity—Eq. 2.20) governed by the water depth.

The height of the tidal wave (H_o) is defined as the difference in the elevation between the highest level (crest) and lowest level (trough), indicated by HW and LW (Fig. 2.5). The distance between two consecutive crests and lows is the wave length (λ) and the time interval of the propagation of these events (tidal cycle) one or two times per day is the tidal period (T_P). The tidal height varies periodically according to the gravitational intensity, and the time interval of these cycles is approximately equal to 12.4 and 25.0 h (semi-diurnal or diurnal, respectively). The highest (higher HW) and lowest (lower LW) tidal wave amplitude occurs when the Earth, Sun and the Moon are aligned or in quarter, respectively (Fig. 2.5).

The tidal amplitude (η_0) is the difference between the crest level (or high water) and the mean sea level, equal to the half of the height ($\eta_0 = H_o/2$). The tidal height in the open sea is usually less than one meter. However, in crossing the continental shelf, or in semi-closed coastal regions, such as bays, inlets and estuaries, there will be amplification of the tidal height which may reach heights of several meters.

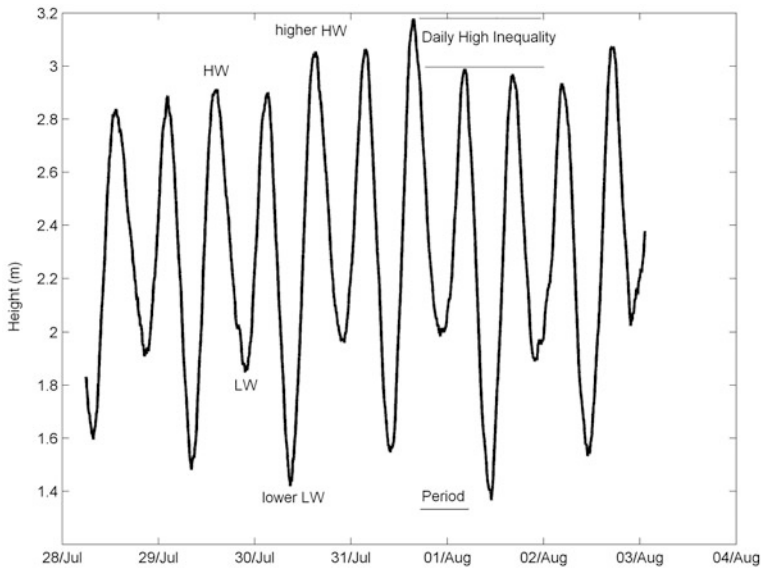


Fig. 2.5 Periodic oscillations of the tide in the Estuarine-lagoon system of Cananéia (Fig. 1.5) showing the high (HW) and low (LW) water oscillations, the corresponding higher HW and lower LW heights, the daily high inequality and the tidal period

Thus, according to the maximum height (H_{MAX}), estuaries are forced by tides which may be classified as (Davies 1964):

Microtide: $H_{MAX} < 2$ m.

Mesotide: $2 < H_{MAX} < 4$ m.

Macrotide: $4 < H_{MAX} < 6$ m.

Hypertide: $H_{MAX} > 6$ m.

The tidal height importance is related to the fact that the periodic tidal inundated areas that may have favorable conditions to the development of vegetation, such as *mangroves* and *salt marshes*. The importance of tidal range lies in the fact that these intertidal habitats will occur only in areas which can be submerged by the tide. Because the highest elevations are only covered for a short time period around high tide, they receive less sediment and nutrients than other areas lower down. Hence, the higher the vegetation, the less nutrients it receives and the slower will be the rate at which it accretes; this has been confirmed by studies performed in the Severn estuary (England) by French (1997).

The tidal prism (T_{PR}) is defined as the sea water volume input into the estuary during the flood tide (from low to high tide), and is related to the tidal height. It may be approximately calculated as $T_{PR} = H_o A_s$, where A_s is the surface area of the estuary. In microtidal regions, the capacity of the water renewal during the tidal cycle is small when compared with estuaries forced by hypertides.

To establish the relative importance of the tidal forcing and the river discharge, a dimensionless number was defined as the ratio of the volume of the fresh water discharge into the estuary during a tidal cycle ($R = Q_f T_P$), and the tidal prism (T_{PR}). This dimensionless number, $F_R = R/T_{PR}$, is named *flux ratio*. Then, according to this definition, when $F_R > 1$ or $F_R < 1$ the estuary is dominated by the river discharge or the tide, respectively. An alternative method to calculate the flux ratio will be presented at the end of this chapter, and as will be seen in Chap. 3, this number has also been used as a criterion for estuary classification.

Besides the dominant semi-diurnal and diurnal tidal oscillations, the tide has components of higher periods: fortnightly and seasonally are the main oscillations. The fortnightly period is the time between successive spring tides and is modulated by Moon phases; this period is 14.8 days, which is the period of maximum constructive interference between the main semi-diurnal tidal constituents M_2 and S_2 , which reinforce at spring tides and are in opposition at neap tides (Leblond and Mysak 1978). Its basic modulation features in shallow rivers were explained through scaling arguments, which show that this wave is generated by the fortnightly modulation of frictional forces due to the variation in tidal velocities (Leblond 1979). There is also a fourth level of height fluctuations, which occurs over longer periods (18.6 years). This oscillation, with frequencies lower than the more energetic ones (semidiurnal and diurnal), are in the sub-tidal domain.

The time variability of the tidal height during events of spring and neap tide, sampled in the estuarine channel of Cananéia (São Paulo State, Brazil), is presented in Fig. 2.6. This figure clearly shows the fortnightly tidal modulation, and the occurrence of the highest and lowest tidal heights during spring and neap tide ($H_o \approx 2.0$ and 0.8 m, respectively), and the sub-tidal oscillation. The high frequency oscillations of temperature simultaneously recorded are coherent with the tidal oscillation, indicating the advective influence of the tidal current in the redistribution of the heat concentration. The low frequency variations of tide and temperature, calculated with a low frequency filter to eliminate the periodic and high energetic variations, are also shown in Fig. 2.6.

The physics of the tidal oscillations decomposition in its components is very complex, being related to the relative motions of the Earth-Sun-Moon system, and may be found in specialized books (Defant 1960; von Arx 1962; Franco 1988, 2009, and others). There is another important aspect related to the tidal wave propagation into the estuary: in this environment, the tidal wave may be composed of short period harmonic oscillations generated by the local topography, the tidal excursion is blocked up by the river discharge and, simultaneously, the tidal wave may be subjected to an energy loss due to the frictional drag in the estuary bottom and margins. Consequently, the tidal wave propagation up and down the estuary undergoes significant modification and substantially deforms, as for instance, in generating the tidal bore.

The interaction between the up estuary tidal wave propagation and the estuary morphology is responsible for the variations in the tidal height and current intensities. Convergent margins of the estuary forces the tidal wave to be laterally compressed and, in the absence of friction, there will be an increase in its height due

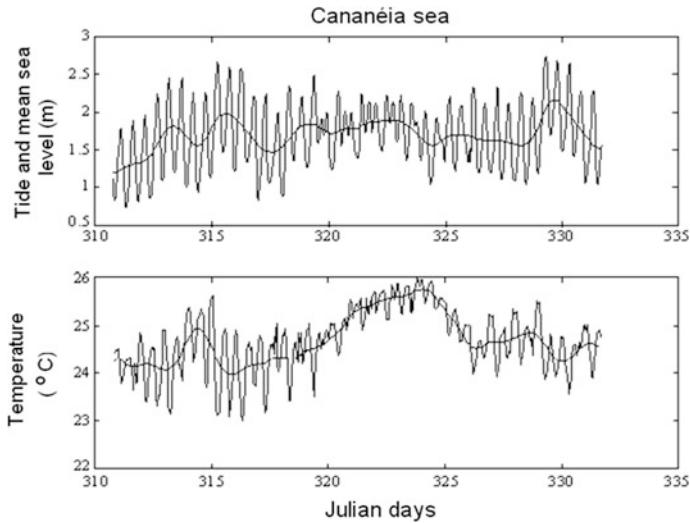


Fig. 2.6 Tidal record in the Lagoon System of Cananéia (southern São Paulo State) showing high and low frequency time variations modulated during spring and neap tides, and the corresponding temperature variations. Time scale in Julian days

to the energy conservation. Inversely, due to the frictional influence, there will be a decrease in the tidal height (Dyer 1997). According to the relative influence of the geometric characteristics of the estuarine channel, the following conditions may be found (Nichols and Biggs 1985; Dyer 1997): (a) hypersynchronous, (b) synchronous and (c) hyposynchronous estuaries.

- (a) Hypersynchronous: convergence exceeds friction and, consequently, the tidal range and tidal currents increase up-estuary until the tidal river zone (TRZ), where convergence diminishes, friction becomes the larger effect and the tide height reduces. These estuaries are generally funnel shaped.
- (b) Synchronous: friction and convergence have equal and opposite effects on the tidal height, and range is constant along the estuary until the river zone (TRZ) is reached.
- (c) Hyposynchronous: friction exceeds the effects of convergence, and the tide range diminishes throughout the estuary. These estuaries tend to have restricted mouths, with the water entering through the mouth effectively spreading out within the estuary. The highest velocities occur at the mouth.

In the northern Brazilian coast hypersynchronous conditions may be observed in shallow estuarine channels in the spring tide and autumn-winter transitional period, with an increase in the tidal height sufficiently large to produce a tidal bore. This occurrence was observed in the Mearim river located in the São Marcos Bay (Maranhão, Brazil), and analyzed in the article of Kjerfve and Ferreira (1993). In this semi-diurnal tidal region the time intervals between flood and ebb have an

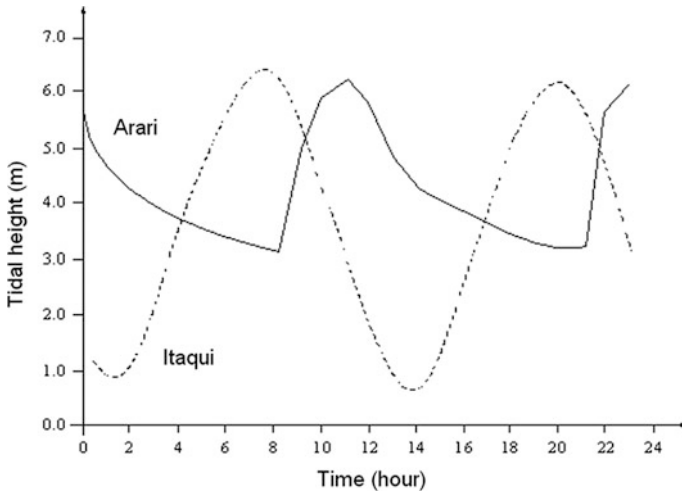


Fig. 2.7 Comparison of the tide forecast in the Mearin River (Maranhão State, Brazil) in Itaqui, and the tide record in Arari, on August 21, 1990. The sinuous sea level macro oscillation in Itaqui, contrasting with the amplitude damping and asymmetric oscillation in Arari (**bold line**) (according to Kjerfve & Ferreira 1993)

asymmetrical behavior, as observed in the simultaneous records of the estuary mouth and up-estuary in the Arari community (Fig. 2.7). The comparative analysis of these records indicates that the sinuous variation changes to a very asymmetric oscillation, indicating a hyposynchronous condition, with time intervals of flood and ebb being 4.0 and 9.0 h, respectively. This indicates, as we will see later, the *flood dominance* phenomenon.

The phenomenon of diurnal inequalities has also been observed in the Santana harbor (Pará, Brazil) located in the left margin of the North Channel of the estuarine delta of the Amazon river, where the time intervals of flood and ebb were 4.0 and 8.0 h, respectively, and similar to the observations in the Mearin River. A simple physical interpretation of this phenomenon, taking into account the propagation of a progressive wave in a shallow channel, will be presented in Chap. 8.

In the shallow water of estuaries, two processes affect the tidal wave propagation. In the first process, even in a frictionless estuary, when the tidal variation of the water depth is large, the wave crest will move more quickly than the trough. The crest of the tide may partially overtake the trough, resulting in a shorter flood and longer ebb; the highest velocities thereby occur in the flood tide. The second is the effect of the bottom friction. This is a non-linear process which depends on the square of the current velocity and its effect is to produce greater friction in shallow water. This also slows down the water movement more at low water levels relative to high water levels. Thus the time delay between low water at the mouth and that at the head is greater than the time delay of the high water. The combined effects of these two processes produces a short duration of the flood phase of the tide and the fast flood currents, creating what is known as *flood dominance*, which has hypersynchronous characteristics. *Ebb*

dominance can also be produced within estuaries, essentially through interactions between deep channels and shallow water areas, and the varying distribution of friction during the tide (Dyer 1997).

The knowledge of tide asymmetric behavior is very important to estuary management, particularly in relationship to the sediment erosion, transport and deposition, as indicated in the analysis of French (1997):

The tide moves a set amount of water into and out of an estuary during each tidal cycle. If the flood and ebb tides are of unequal length, then in the shorter tide, the fixed volume of water has to move faster than in the longer tide. That is, if the flood tide takes 4.0 h and the ebb takes 8.0 h, then the estuary has, in effect, 4.0 h to fill and 8.0 h to empty. The only way that this can be achieved is by variations in velocity and, therefore, energy. If, as in the situation above, flood periods are shorter, and energy greater, more sediment can be carried in on the flood tide than can be moved out on the ebb tide (assuming adequate sediment supply). Hence, the estuary will experience a net input of sediment. In contrast, if the situations were reversed, and the flood tide took longer than the ebb, there would be greater velocities and greater energy during the ebb, and, therefore, more sediment moved and a net sediment loss to the system. This net movement of sediment is also modified by other factors, such as residual currents, the mechanism of sediment transport (bedload or suspension), sediment stability, and sediment entrapment.

With the development of the classical method of Doodson (1928) to the analysis, the astronomic tidal height forecast and the techniques using spectral analysis (Franco 1988, 2009), the hourly time series values of the tidal height measurements are able to be decomposed into a set of harmonic components by a computational procedure using the Pacmaré (Franco 2000); this program performs analyses for long periods (18.6 years) and shorter periods (1 year or less). The theoretical foundation of the classical tidal harmonic analysis has also been presented by Pawlowicz et al. (2002), and complemented with a set of programs written in MATLAB® to perform analyses for periods of one year or shorter. The main components are semidiurnal and diurnal, which take into account about 83% of the total tidal amplitude. Some of these components are presented in Table 2.1, with its amplitudes and phase values determined from a 30 day time series of hourly tidal height records in the Bertioga estuarine channel (São Paulo, Brazil).

Table 2.1 Harmonic constants (amplitude and phase) of the main tidal components in the Bertioga estuarine channel, computed according to Franco (2000), using a 30 days of hourly measurements

Diurnal components	Amplitude (cm)	Phase (°)
O ₁ —main-lunar	11.2	27.5
K ₁ —lunar-solar	6.9	189.5
P ₁ —main-solar	6.3	109.0
Semi-diurnal components	Amplitude (cm)	Phase (°)
M ₂ —main lunar	32.6	174.9
S ₂ —main solar	23.5	184.3
N ₂ —lunar-elliptic	5.6	240.5

The relative importance of diurnal and semidiurnal tidal components may be obtained with the *form number* (N_f) defined by A. Courtier in 1938 (quoted by Defant 1960), by the following ratio:

$$N_f = \frac{K_1 + O_1}{M_2 + S_2}, \quad (2.7)$$

where K_1 , O_1 , M_2 and S_2 are the main diurnal (index 1) and semidiurnal (index 2) tidal components. According to the variation of this dimensionless number the tide may be classified as:

$0 < N_f < 0.25$ —semidiurnal;

$0.25 < N_f < 1.5$ —mixed, with semidiurnal predominance;

$1.5 < N_f < 3.0$ —mixed, with diurnal predominance;

$N_f > 3.0$ —diurnal.

Using this classification criteria the tidal oscillation in the Bertioga estuarine channel is $N_f = 0.32$, classified as mixed, with semidiurnal predominance (Miranda et al. 1998).

The co-oscillating tide at the estuary mouth propagates up-estuary as a shallow water wave, because its length is too great in comparison to the estuarine depth. The horizontal motions associated with the tidal oscillations are named *tidal currents*. These motions undergo significant modification due to the frictional drag, morphology, relative vorticity and also by the Earth's rotation due to the Coriolis acceleration; this last influence is more evident in estuaries with great dimensions and forced by diurnal tides. When the natural oscillation period of the water body of the estuarine system is equal or close to the main tidal component, the resonance phenomenon may be observed, and the height of the stationary wave may reach several meters. Classic examples are its occurrence in the Bay of Fundy (Gulf of Maine, USA) and the Igarapé do Inferno in the Amazon continental shelf (Brazil). In this condition, the tidal prism (T_{PR}) is very large compared with the estuary volume in low tide, and the water mass renewal in the estuary is efficient in removing unwanted wastes.

In theoretical problems when the tide variation must be taken into account, it may be convenient to simplify the theory by considering this forcing to be analytically represented by only one tidal component as:

$$\eta(x, t) = \eta_0 \cos(\kappa x - \omega t), \quad (2.8)$$

where $\omega = 2\pi/T$ and $\kappa = 2\pi/\lambda$ denote the angular frequency and the wave number, respectively. This equation may be, for instance, used as a boundary condition to simulate the tidal forcing at the estuary mouth.

2.3 Dimensional Analysis Applied to Equations and Processes

Although simple uses of this technique have already been given in this chapter, the application of *dimensional analysis* is very useful in theoretical development of complex and non-complex processes, and to check the correctness of its intermediate and final results. As an introduction to this approach, let us consider some definitions of non-dimensional parameters already given and a physical problem related to the main forces which drives the estuarine processes.

In dimensional analysis, the dimension of a quantity is denoted by square brackets [] and is expressed in reference to the fundamental quantities of Physics: mass (M), length (L) and time (T). As simple examples of applying this analysis let us take as first the already defined tidal prism $T_{PR} = H_o A_s$, which is a volume $[L^3]$ which depends on the product of tidal height (H_o) and the estuary surface area (A_s); then the dimension of T_{PR} are: $[T_{PR}] = [LL^2]$, which may also be abbreviated by $[T_{PR}] = [L^3]$, and the water volume R discharged by the river discharge (Q_f) into the estuary during the time interval of one tidal period (T_p) is calculated by $R = Q_f T_p$ and $[R] = [L^3 T^{-1} T] = [L^3]$. The ratio of these quantities (T_{PR}/R) was defined as the *flux ratio* (F_R) which, is a non-dimensional quantity, as well as, the form number N_f (Eq. 2.7).

In the next topic of this chapter we are going to deal with the *gradient pressure force* in terms of acceleration, that is, force per unit of mass, which has two main components: the barotropic and the baroclinic, whose dimensions are,

$$\left[g \frac{\partial \eta}{\partial x} \right] = \left[L T^{-2} \frac{L}{L} \right] = [L T^{-2}],$$

and,

$$\left[\frac{g}{\rho} \int_z^\eta \frac{\partial \rho}{\partial x} dz \right] = \left[\frac{L T^{-2}}{M L^{-3}} \frac{M L^{-3}}{L} L \right] = [L T^{-2}].$$

Another example of using dimensional analysis will follow from the steady-state equation of motion of a well-mixed and laterally homogeneous estuary, forced by the barotropic and baroclinic components of the gradient pressure force. Under the assumption of a constant kinematic eddy viscosity coefficient (N_z), this equation may be written as (Eq. 10.4, Chap. 10),

$$\frac{\partial^2 u}{\partial z^2} - \frac{g}{\rho N_z} \frac{\partial \rho}{\partial x} z + \frac{g}{N_z} \frac{\partial \eta}{\partial x} = 0.$$

The general solution of this second order differential equation is dependent on two integrations constants (C_1 and C_2), which may be calculated under specified upper and lower boundary conditions,

$$u(x, z) = \frac{1}{6} \frac{g}{\rho N_z} \frac{\partial \rho}{\partial x} z^3 - \frac{1}{2} \frac{g}{N_z} \frac{\partial \eta}{\partial x} z^2 + C_1 z + C_2.$$

The dimension of the first member of this equation is $[LT^{-1}]$, and for first and second terms on the right-hand-side, the analytical expression and the corresponding dimensions are:

$$\left[\frac{1}{6} \frac{g}{\rho N_z} \frac{\partial \rho}{\partial x} z^3 \right] = \left[\frac{LT^{-2}}{L^2 T^{-1}} \frac{L^3}{L} \right] = [LT^{-1}],$$

and

$$\left[\frac{1}{2} \frac{g}{N_z} \frac{\partial \eta}{\partial x} z^2 \right] = \left[\frac{LT^{-2}}{L^2 T^{-1}} L^2 \right] = [LT^{-1}],$$

which indicates that the analytical expressions of these terms, as would be expected, have dimension of velocity.

The analytical expressions of the constants C_1 and C_2 , obtained by applying the boundary conditions, will have a correct analytic expressions if $[C_1] = [T^{-1}]$ and $[C_2] = [LT^{-1}]$, which may be easily checked. Further examples on the application of dimensional analysis to physical and biological problems may be found in the book edited by Platt et al. (1981).

2.4 What Generates the Circulation and Mixing in the Estuary?

To answer this question, which we judge important in this chapter, it is necessary to use some fundamental concepts and the hydrodynamic equations of sea water, which are studied in others areas of Physical Oceanography, and will be presented in detail under the optics of estuarine physics in Chaps. 7 and 8.

The estuary dimension vary between small and medium spatial scales, in relation to the adjacent ocean, and for most estuaries their lengths (L) is much greater than their width (B). Between the estuary head and mouth, the salinity varies between the fluvial water (salinity practically zero), and that of the coastal region (S_o), generating a mean longitudinal salinity gradient ($\Delta S/\Delta x$) equal to S_o/L .

The geometric estuarine characteristic has a great influence on its motions and on the distribution of properties, which are often studied using a right-handed rectangular Cartesian co-ordinates system Oxyz (Fig. 2.8a); the origin being in the mean level of the free surface. Oxy plane is located on the free surface and

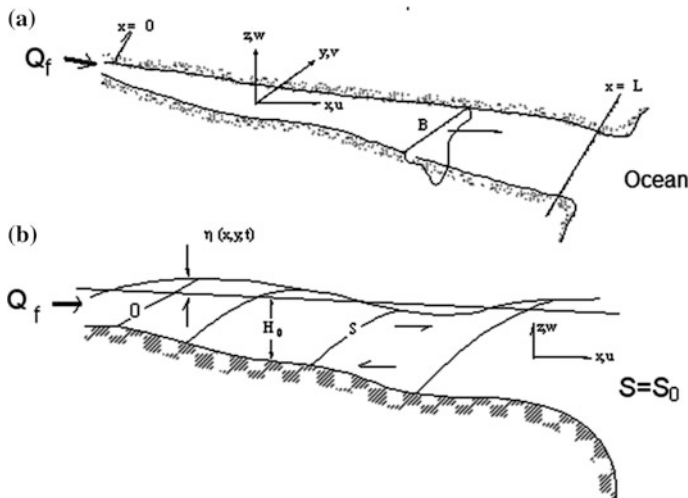


Fig. 2.8 **a** Scheme of a coastal plain estuary indicating the Oxyz reference system, the u , v , w velocity components, the cross section with width B and the river discharge Q_f . **b** The longitudinal section with the isohalines, S , the co-oscillating tide, $\eta(x, y, t)$, and the depth $H_0(x, y)$. The Oz axis is oriented against the acceleration of gravity

orthogonal to the gravity acceleration, the Ox axis is usually oriented longitudinally in the positive sense seaward (or eventually landward), the Oy axis, indicating the transverse estuary dimension, is perpendicular to the Oxz plane and the Oz axis vertically upwards will be oriented against, or in the same sense of the gravity acceleration. The velocity components, in relationship to the coordinate axis, are denoted by u , v , and w , respectively; the components u and v are denominated longitudinal and transversal (or secondary), respectively.

In the estuary longitudinal section (Fig. 2.8b), the Oxz axes indicates the longitudinal and depth characteristics of the salinity field by its isohalines distribution ($S = \text{const.}$). This figure also indicates that the estuarine water mass is also forced by the tidal co-oscillation in the longitudinal direction, and its height variation is denoted by $\eta = \eta(x, y, t)$.

The motions in this transitional coastal environment are generated by the following forcings: sea level variations, freshwater discharge, gradient pressure force (due to the thermohaline influence on the density), continental shelf circulation and wind stress acting on the free surface. These forcings are functions of time and space and simultaneously act on the estuarine water body. The circulation on the continental shelf is mainly driven by the wind stress; its influence, generating the circulation and mixing processes may be observed on synoptic and seasonal time and space scales. Our study is restricted to the conditions found in the majority of coastal plain estuaries, and we will examine the motions generated by: the co-oscillating tide, $\eta = \eta(x, y, t)$, the fresh water discharge, Q_f ; and the longitudinal salinity ($\partial S / \partial x$) or density ($\partial \rho / \partial x$) gradients.

The time scale of the estuarine water body to the impulsive forces is large, and usually separated in motions in the dominium of high and low frequency. The dilution of the sea water by the freshwater of the river discharge will also produce variations in the longitudinal salinity gradient that will contribute to the estuary's dynamic structure.

The various dynamic physical mechanisms that generate the estuarine circulation and control the salinity distribution and the chemical, biological and geological properties are liable to a hydrodynamic formulation. This formulation will be presented later using tools of the geophysical fluid dynamics, aiming to forecast its motions, the water interchanges with the adjacent ocean and the physical characterization of the estuary.

As the oscillation periods of the co-oscillating tide are well known, it is possible to separate the effects of the low frequency forces using a statistic procedure of experimental data. Theoretically, this separation is made with the integration (from the generic depth z , at a pressure p), up to the free surface η (submitted to the atmospheric pressure $p = p_a$) of the fundamental hydrostatic equation ($\partial p / \partial z = -\rho g$ or $\partial p = -\rho g dz$) with the Oz axis oriented according to Fig. 2.8,

$$p_a - p = -g \int_z^{\eta(x,t)} \rho dz. \quad (2.9a)$$

To calculate the longitudinal pressure gradient, the expression (2.9a) must be derived in relation to x , and applying to the term in the right-hand-side the Leibnitz rule of the derivation of an integral, because its upper integration limit $z = \eta(x, y, t)$ is function of x , and the result is:

$$\frac{\partial p_a}{\partial x} - \frac{\partial p}{\partial x} = -g(\rho_\eta \frac{\partial \eta}{\partial x}) + \left(\int_z^{\eta(x,t)} \frac{\partial \rho}{\partial x} dz \right). \quad (2.9b)$$

Then, calculating from this expression the longitudinal components of the pressure gradient force per mass unity, which generate motions oriented from high to low pressure regions, is obtained by multiplying by the factor $(-1/\rho)$ all terms of Eq. (2.9b),

$$-\frac{1}{\rho} \frac{\partial p}{\partial x} = -\frac{1}{\rho} \frac{\partial p_a}{\partial x} - g \frac{\partial \eta(x, t)}{\partial x} - \frac{g}{\rho} \int_z^{\eta(x,t)} \frac{\partial \rho}{\partial x} dz, \quad (2.9c)$$

With the approximation $\rho_\eta / \rho = \rho_o / \rho \approx 1$. All terms of Eq. (2.9c) have dimension of acceleration (force per mass unity) and, in the right-hand-side we have the following longitudinal components of the pressure gradient force: the barometric, the barotropic and the baroclinic, respectively.

Lets us consider some simple solutions of the Eq. (2.9c), under steady-state condition and at the sea surface, $z = \eta(x)$, then, it is reduced to

$$0 = -\frac{1}{\rho} \frac{\partial p_a}{\partial x} - g \frac{\partial \eta}{\partial x}. \quad (2.9d)$$

Solving this equation by finite increments to the estuary free surface elevation $\Delta\eta$, it follows that:

$$\Delta\eta = -\frac{1}{\rho g} \Delta p_a. \quad (2.9e)$$

This result indicates that for an increase of the atmospheric pressure ($\Delta p_a > 0$), the sea surface responds as an inverted barometer, because $\Delta\eta < 0$, and the following order of magnitude may be estimate: for an increase (decrease) of the atmospheric pressure of $1.0 \text{ mbar} = 10^2 \text{ N m}^{-2}$, the sea surface is depressed (elevated) by 0.01 m . However, in nature, the static influence of low atmospheric pressure centers are usually related to the low frontal zones propagations, that may reaches the coastal regions with strong winds, and the association of these influences (static and dynamic) may generate dangerous storm-surges at the coastline.

As the salinity influences on the density is predominant over the pressure (p) and temperature (T), the longitudinal density gradient in Eq. (2.9c) may be substituted by the corresponding longitudinal salinity gradient ($\partial S/\partial x$), calculated using a linear simplified equation of state, $\rho(S) = \rho_o(1 + \beta S)$ (Eq. 4.12, Chap. 4), where ρ_o is a constant density value, and β is the mean saline or haline contraction coefficient, define by $\beta = (1/\rho)(\partial \rho/\partial S)$. However, this coefficient varies with the S , T and p properties, but for estuarine water mass this coefficient may be approximate by a constant value ($\beta \approx 7.5 \times 10^{-4} (\%)^{-1}$). With these simplifications, and disregarding the barometric pressure gradient, the longitudinal component of the pressure gradient force, per mass unity has the following expression:

$$-\frac{1}{\rho} \frac{\partial p}{\partial x} = -g \frac{\partial \eta}{\partial x} - \frac{g}{\rho} \int_z^\eta \frac{\partial \rho}{\partial x} dz, \quad (2.10a)$$

or

$$-\frac{1}{\rho} \frac{\partial p}{\partial x} = -g \frac{\partial \eta}{\partial x} - g\beta \int_z^\eta \frac{\partial S}{\partial x} dz. \quad (2.10b)$$

It should be noted that in the article published in 1952 (Pritchard 1952), D.V. Pritchard became the first researcher to link estuarine circulation to the forcing by horizontal density gradient, using observations from the James river estuary (Virginia, USA) to demonstrate this mechanism (quoted in Geyer 2010, p. 13).

The first parcel on the right-hand-side of Eq. (2.10a) indicates that the dynamic influence generated by the tidal forcing is independent of the depth (barotropic), and its intensity is proportional to the negative value of the sea surface slope. In estuaries, the time variations in the velocity intensity sequentially assume the following trend: when $\partial\eta/\partial x > 0$, reach maximum landward intensity at the mid-flood tide, the velocity decreases to zero at high and low tide ($\partial\eta/\partial x = 0$), before reversing ($\partial\eta/\partial x < 0$) to maximum ebb velocity midway through the ebb, where almost zero intensity is reached closing the tidal cycle.

For an estuary with a length of 10^4 m (10 km), forced by meso-tidal oscillation ($2 < H_0 < 4$ m), the maximum intensity, per mass unity may be estimated as varying between -10^{-3} and 10^{-3} m s $^{-2}$, in the flood and ebb tide, respectively. Then, this gradient force component varies in the interval -10^{-3} to 10^{-3} m s $^{-2}$, with the null intensity occurring at high and low tide.

The dynamical influence of the distribution of the longitudinal density (salinity) gradient is proportional to the longitudinal density gradient, integrated in the interval from the depth z up to the free surface level, $\eta = \eta(x, y, t)$, (Eqs. 2.10a). Its intensity is zero at the free surface ($z = \eta$) and increases with depth, but its value is always negative because the density (salinity) increases seaward $\partial\rho/\partial x > 0$ ($\partial S/\partial x > 0$). The dynamical influence of this component of the gradient force (baroclinic), per mass unity, always generates landward (flood) motions; its intensity increases with depth, and its maximum value is on the bottom. For an estuary with a length of 10^4 m (10 km), a mean depth of 10 m, and a longitudinal salinity variation from zero to 30‰ at the head and mouth, respectively, its maximum intensity may be estimated as a relative value of -10^{-4} m s $^{-2}$. Hence, the intensity of this component varies in the interval -10^{-4} m s $^{-2}$ to 0, with zero at the surface. Then, according to these estimated intensities of the baroclinic pressure gradient component, which always generates landward or flood motions, its maximum value is 10 times less than the modulus of the barotropic component. However, its intensity will be higher than the barotropic component near the slacken water.

The river discharge (Q_f), besides to diluting the sea water and generating a longitudinal density gradient, is also responsible for another low frequency component that generates velocity in the estuarine water mass. However, in opposition to the baroclinic component, the mean steady-state value of this component (u_f) always generates seaward motion. By the volume integrated mass conservation principle, the intensity of this component is given by the following ratio:

$$u_f(x) = \frac{Q_f(t)}{A(x)}, \quad (2.11)$$

where $A = A(x)$ is the mean area of a transversal section during the tidal cycles. The time variation of this velocity component (u_f) is dependent on the low frequency variations (usually seasonal) of the river discharge.

Under steady-state conditions the tidal oscillation vanish and so the barotropic pressure gradient, and the resulting low frequency motion forced by the

Table 2.2 Vertical profiles of the intensity and direction of the current (velocity vector) measured in the Cananéia estuarine channel, at two different times, t_1 and t_2 of ebb tide

Depth (m)	Vel. (m s^{-1}) (t_1)	Direction ($^\circ$) (t_1)	Vel. (m s^{-1}) (t_2)	Direction ($^\circ$) (t_2)
0.0	1.09	201	0.22	198
1.0	1.09	188	0.21	187
2.0	0.94	187	0.10	199
3.0	0.85	191	0.02	168
4.0	0.74	197	0.19	011
5.0	0.59	198	0.30	024
6.0	0.44	175	0.33	010
7.0	0.30	172	0.47	017

longitudinal baroclinic pressure gradient of density and by the river discharge in landward and seaward direction, respectively, forces to generate a two layer bidirectional motion. This motion is named *gravitational circulation*, *gravity current* or the *classical estuarine circulation*. It is essentially a two dimensional advective motion which drives the volume and salt transports seaward and landward in the upper and lower layers, respectively.

To illustrate the dynamics effects of the barotropic and baroclinic pressure gradients in the velocity components, experimental data are presented in Table 2.2. These vertical velocity profiles were measured in the estuarine channel of Cananéia sea (Fig. 1.5, Chap. 1), in two times (t_1 and t_2) of the ebb tide, in the position where the channel is oriented in the north-south direction.

The experimental data indicate that in the vertical profile at time t_1 , the estuarine circulation is southwards (seaward) with direction between 172° and 201° , and with relatively high speeds from 0.30 to 1.09 m s^{-1} . This physical characteristic indicate that during this ebbing event the barotropic gradient component of the pressure gradient force prevailed over the baroclinic component. In the following instant (t_2), the velocity minimum is 0.02 m s^{-1} at 3 m depth; in this layer between the surface and 3 m depth, the motion is also southward (direction between 168° and 199°), but with very low intensities ($<0.22 \text{ m s}^{-1}$) compared to the preceding profile (t_1). At depths bellow 3 m, the intensity increases, but the circulation is in the opposite direction (landward) to the upper layer, as indicated by its direction from 11° to 24° . These results indicate that the water column, with only seven meters depth, has bidirectional circulation during the ebbing tide, with the non-motion depth at the middle of the water column ($\approx 3 \text{ m}$). Then, with the decrease in the intensity of the barotropic component of the pressure gradient force, there was an increase in the relative importance of the baroclinic pressure gradient in the deepest layers of the estuarine channel. As demonstrated in this experiment, the baroclinic component of the pressure gradient force always generates landward circulation, and its intensity increases with depth (second term on the right-hand-side in Eq. 2.10).

The motions described in the preceding paragraphs are macroscopic, usually named as advective, to distinguish them from the microscopic or small-scale motions that generate turbulent diffusion. In the following paragraphs, the influence of the

microscopic motions in the redistributions of properties in the estuarine water mass by *mixing process* (advection and diffusion) will be examined. Focusing our attention on one volume element of control, the local salinity variation ($\partial S/\partial t < 0$ or $\partial S/\partial t > 0$) indicates the occurrence of salt dilution (or the salt concentrate)—dilution by the river water and concentration by the seaward input. This process is a simple description of the mixing between water masses. Salinity was used as an indicator, but this process is generated by the salt transport due to the macroscopic motion (advective) and the simultaneous microscopic flux of properties due to: interchanges of kinetic energy, heat, salt and contaminants introduced in the estuary. These fluxes of properties are due to the following motions:

- (a) Macroscopic or medium motion (generated by the tide, river discharge and density gradients); this process contributes to the mixing and is named *advective*;
- (b) Microscopic and random motions, whose effects on the mixing are denominated as *molecular* or *turbulent diffusion* in laminar and turbulent motions, respectively.

The advective influence changing the salinity concentration during the tidal cycle is evidenced in the comparison of the u-velocity component and vertical salinity profiles (Fig. 2.9a, b), which were simultaneously sampled at half-hourly time intervals during a semi-diurnal tidal cycle. The turbulent diffusion generates the erosion of the vertical salinity variation shown in the salinity profiles from 31.0 and $\approx 36.0\text{‰}$ (Fig. 2.9a), which migrate in the water column due to the velocity intensity variation. This process is due to the turbulent mixing generated by internal friction water layer with different intensities, and the estuary friction at the bottom. The layer with the higher vertical salinity gradient is called *halocline*, although in oceanic water this term is used to indicate a salinity decrease with depth.

The time variability of the u-velocity profiles during the ebb ($u > 0$) and flood ($u < 0$) is shown in Fig. 2.9b. The ebbing intensities ($\approx 0.6 \text{ m s}^{-1}$) are higher than in the flood ($\approx -0.3 \text{ m s}^{-1}$), due to the influence of the barotropic gradient pressure force and the river discharge. This asymmetry, when analysed in terms of steady-state mean values, indicates the presence of the river discharge and the influence of the barotropic pressure gradient. It should be also pointed out, that this figure also indicates the influence of the baroclinic pressure gradient in the bi-direction characteristic of the vertical velocity profiles in the neighborhood of the HW and LW tides when the barotropic forcing tends to zero.

By analogy with the tide, the circulation variability in estuaries is classified as *intertidal* when it occurs at semi-diurnal or diurnal tidal frequencies (>1 cycle/day), or *subtidal* at lower frequencies (<1 cycle/day). The main subtidal frequency is the fortnightly, and is due to the time period modulation between successive spring tides (≈ 15 days).

The longitudinal salinity advective flux (ϕ_{adv}) and the diffusive flux (ϕ_{dif}) fluxes, associated with the macroscopic (mean) and the turbulent (microscopic) motions,

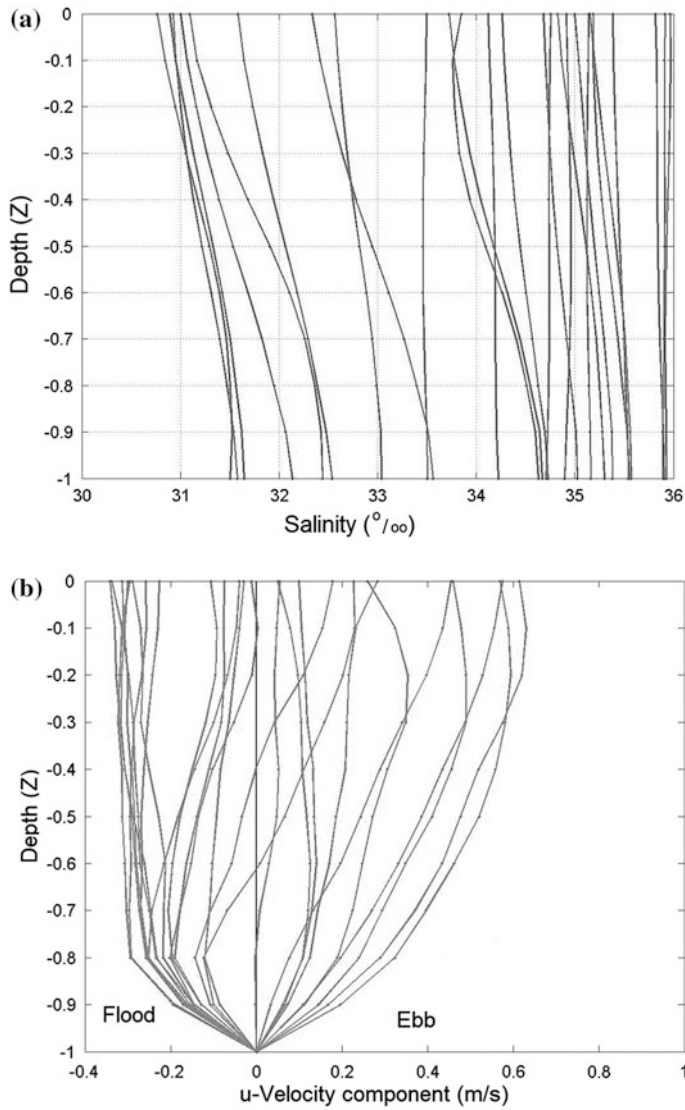


Fig. 2.9 Time variability of half-hour vertical profiles of salinity (a) and the u-velocity component (b) during a complete semidiurnal tidal cycle. Positive and negative velocity values indicate flood and ebb, respectively, and Z is the non-dimensional depth (after Andutta 2011)

are defined by: $\phi_{adv} = \rho S u$ and $\phi_{dif} = -(\rho K_{xs}) \partial S / \partial x$, respectively; these fluxes have both dimensions of $[ML^{-2}T^{-1}]$. The coefficients K_{xs} and ρK_{xs} are the kinematic and dynamic eddy diffusion coefficients of salinity, with dimensions $[K_{xs}] = [L^2T^{-1}]$ and $[\rho K_{xs}] = [ML^{-1}T^{-1}]$. The formulation of the diffusive flux is parameterized with the Fickian law, and is oriented from the regions of high

concentration to lower concentration. In the SI system of unit these fluxes are expressed in $\text{kg m}^{-2} \text{s}^{-1}$. The equivalent expressions may be written for concentration of any property, using the corresponding diffusion coefficients.

2.5 Tidal Wave Propagation in an Estuary

The tidal wave propagation in estuaries involves a relatively intense advective process, usually in a region with complex topography. Some of the inter-connected features are the phase and the related phase differences of the wave propagation, tidal current and salinity variations, the tidal excursion and length of the saline intrusion. The most elaborated theory of tidal wave propagation in a channel, taking into account the most important characteristics, was developed in the pioneering paper of H. Poincaré, in 1910. The dynamics of the tidal currents were studied by Fjeldstad (1929), taking into account the bottom frictional forces (quoted in Defant 1961).

It follows a classical and simplified solution for the wave propagation in estuaries, according to Defant (1960), Ippen and Harleman (1961), Dyer (1973) and others, that is useful to illustrate the physical processes occurring in estuarine channels, although of limited interest because it uses a simple geometry (long channel and rectangular transverse section), and doesn't take to account the non-linear dissipative frictional forces, it is a useful approach on the wave propagation in channels.

As by hypothesis the estuary depth is small when compared to the wave length of the tidal co-oscillation, the nature of this oscillatory motion is that of an oscillatory wave in shallow water, which differs in physical behavior from that of a short wave propagation. As the ratio of the water depth (H_0) to the wave length (λ) is much less than one [$(H_0/\lambda) \ll 1$], the solution is reduced to that of a non-dimensional shallow water problem (Pedloski 1979).

The hypotheses applied to the theoretical development are:

- (a) The salinity (density) field is steady and uniform.
- (b) The channel length (L) is less than the wave length ($L < \lambda$).
- (c) Channel long and narrow ($L \gg B$), one-dimensional motion ($v = w = 0$), uniform transversal section, and there is no deflection due to the Earth's rotation (Coriolis acceleration is disregarded).
- (d) With the tidal co-oscillating motion in the channel entrance there is the water storage in the channel during the flood (tidal prism), and the subsequent exit of this water in the ebb.

In order to develop the theory of the oscillating tidal motion, a coordinate system indicated in Fig. 2.10 will be used. The vertical axis (Oz) is oriented positively against the gravity acceleration (\vec{g}) with its origin on a uniform bottom with the

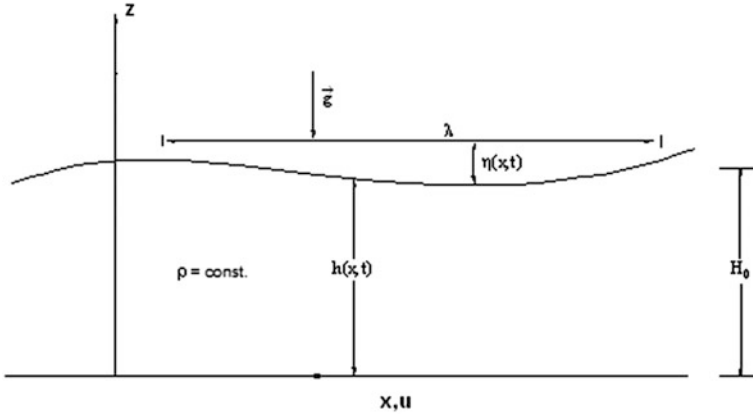


Fig. 2.10 Reference system of a wave oscillation, $\eta(x, t) = h(x, t) - H_0$, in a long shallow water channel of rectangular cross-section. The longitudinal axis Ox is oriented positively in the up-channel direction. The salinity (density) field is steady and uniform

water layer undisturbed, indicated by H_0 . The origin of the horizontal axis ($x = 0$) is located at the estuary mouth and oriented positively in the up-channel direction.

In this development, the simplified equation of continuity and the Ox component of the equation of motion will be used, which are obtained from its tri-dimensional equations with a mathematical procedure which will be presented in Chap. 7 and 8. We will be considering the shallow water approximation. As $\eta = \eta(x, t)$ is the oscillation of the free surface related to the depth, H_0 , and the salinity is constant, the longitudinal component of the gradient pressure force, per mass unity (Eq. 2.10a), is simplified, to the barotropic component,

$$\frac{1}{\rho} \frac{\partial p}{\partial x} = g \frac{\partial \eta}{\partial x}. \quad (2.12)$$

With the indicated simplifications, the equation of motion is reduced to the following one-dimensional expression (Harleman 1971; Pedloski 1979):

$$\frac{\partial u}{\partial t} + u \frac{\partial u}{\partial x} = -\frac{1}{\rho} \frac{\partial p}{\partial x} = -g \frac{\partial \eta}{\partial x}. \quad (2.13)$$

Under the hypothesis that $\eta(x, t) \ll H_0$, this equation may be transformed in a linear equation disregarding the advective acceleration ($u \frac{\partial u}{\partial x} = 0$). Then, it is reduced to:

$$\frac{\partial u}{\partial t} = -g \frac{\partial \eta}{\partial x}, \quad (2.14)$$

which is the simplified expression of the linear shallow water equation, without friction and with the assumption that the Coriolis acceleration is negligible. The unknowns of this equation are the u -velocity component, $u = u(x, t)$, and the sea surface elevation, $\eta = \eta(x, t)$.

Taking into account that the motion is one-dimensional, it is necessary to use the corresponding continuity equation to transform it into a closed hydrodynamic system; for this to be accomplished, the continuity equation has the following analytic expression (Pritchard 1958):

$$\frac{\partial(uA)}{\partial x} + \frac{\partial A}{\partial t} = 0, \quad (2.15)$$

where A is the cross section area, $A = B(H_0 + \eta)$. Combining this area with Eq. (2.15), and performing the derivations in relation to x , it follows:

$$(H_0 + \eta) \frac{\partial u}{\partial x} + u \frac{\partial(H_0 + \eta)}{\partial x} = - \frac{\partial \eta}{\partial t}. \quad (2.16)$$

Taking into account the approximation $\eta \ll H_0$ the equation reduces to:

$$H_0 \frac{\partial u}{\partial x} + \frac{\partial \eta}{\partial t} = 0, \quad \text{or} \quad \frac{\partial(H_0 u)}{\partial x} + \frac{\partial \eta}{\partial t} = 0, \quad (2.17)$$

which is the simplified form of the continuity equation of shallow water. Equations (2.14) and (2.17) form a system of two equations of partial derivatives and two unknowns: the free surface oscillation $\eta = \eta(x, t)$ and the velocity $u = u(x, t)$. The solution of this system of equations, assuming a linear frictional dependence proportional to the u -velocity in the right-hand-side of Eq. (2.14), which dissipates the amplitude of the tidal wave with an exponential decrease, $e^{-\mu x}$, with $(\mu = (\tau/2)\sqrt{gH_0})$, is presented by Blumberg (1975).

Eliminating by cross derivation from Eqs. (2.14) and (2.17) the variables $\eta = \eta(x, t)$ and $u = u(x, t)$, respectively, we have:

$$\frac{\partial^2 \eta}{\partial t^2} = gH_0 \frac{\partial^2 \eta}{\partial x^2}, \quad (2.18)$$

and

$$\frac{\partial^2 u}{\partial t^2} = gH_0 \frac{\partial^2 u}{\partial x^2}. \quad (2.19)$$

This equation set is the classical equations of progressive waves (the wave profile propagates horizontally) in a channel with a uniform transverse section, with a phase propagation velocity (celerity) c_0 expressed by:

$$c_0 = \sqrt{gH_0}. \quad (2.20)$$

A possible solution of Eq. (2.18) is the harmonic function,

$$\eta(x, t) = \eta_0 \cos(\kappa x - \omega t + \Phi), \quad (2.21)$$

simulating the wave propagation in the $x > 0$ direction (landward). Φ is an arch of positive first determination, that is, $0 \leq \Phi \leq 2\pi$, which may be determined by the initial and boundary conditions. If, for example, the surface elevation in the estuary mouth at time $t = 0$ is equal to η_0 , then $\eta(0, 0) = \eta_0$ and, consequently, $\cos(\Phi) = 1$ and $\Phi = 0$. In this case, at the estuary mouth the higher elevation values of the oscillation, $\eta = \eta(x, t)$, will occur at times $t = 0, T, 2T, \dots$ For $x = \lambda$ and any of multiples of this length, the wave will occur in phase with the position at $x = 0$. The simplifying hypothesis generated a symmetric tidal wave. However, in nature, the wave propagation may be greatly distorted, as exemplified for the Mearin river (Fig. 2.7).

As estuaries have a finite length, which is generally small compared to one quarter of the tidal wave length ($L < \lambda/4$), the oscillation of the free surface is usually uniform along the estuarine channel. Due to this behavior, this oscillation may be simulated by $\eta(t) = \eta_0 \cos(\omega t)$, as found in the classical work of Arons and Stommel (1951), when the stationary salinity distribution in an estuary was studied with these characteristics (one dimension, simple geometry and frictionless).

As it is a liner problem, velocity solution (Eq. 2.19) is also analytically represented by the same harmonic dependence:

$$u(x, t) = U_0 \cos(\kappa x - \omega t + \Phi). \quad (2.22)$$

In this solution U_0 is the velocity amplitude, which may be determined by calculating the first derivatives of solutions (2.21) and (2.22) relative to the variables t and x , respectively, and combining this result with the continuity Eq. (2.17), resulting the following relationships: $U_0 = \eta_0 \omega / H_0$. $\kappa = \eta_0 \lambda / H_0 T = \eta_0 c_0 / H_0$, where $c_0 = \lambda / T$ is the phase velocity of the wave. Then, the solution of Eq. (2.22) may be re-written as,

$$u(x, t) = \frac{\eta_0 c_0}{H_0} \cos(\kappa x + \omega t + \Phi), \quad (2.23)$$

or, combining with Eq. (2.21),

$$u(x, t) = \frac{c_0}{H_0} \eta(x, t), \quad (2.24a)$$

or

$$u(x, t) = \eta_0 \sqrt{\frac{g}{H_0}} \cos(\kappa x + \omega t). \quad (2.24b)$$

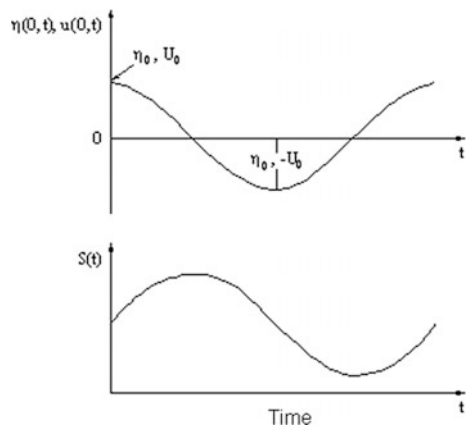
From this result it follows that the amplitude U_0 of the tidal velocity may be approximated by $U_0 = \eta_0 \sqrt{\frac{g}{H_0}}$; for a tidal wave with an amplitude $\eta_0 = 1$ m, and a channel depth of $H_0 = 10$ m $\rightarrow U_0 \approx 1$ m s⁻¹. As will be seen later (Chap. 8) the product of a non-dimensional coefficient k by $U_0 H_0$, may be used to simulate the vertical kinematic eddy viscosity coefficient ($N_z = k U_0 H_0$).

Due to the initial hypothesis this solution is valid for $\eta \ll H_0$ and, from this inequality, it follows that for $\eta_0 \ll H_0$, the amplitude U_0 will always be less than c_0 ($U_0/c_0 \ll 1$). Despite the approximations made to reach the simplified solution it is useful to show a fundamental characteristic of the flow: (i) the u -velocity due to the wave propagation, does not exceed the phase velocity of the proper wave (Mello 1998), and (ii) It may be used to estimate the tidal wave velocity, for example: for a tidal amplitude $\eta_0 = 1$ m propagating in an estuary with 10 m depth the maximum tide velocity will be 1 m s⁻¹.

Equation (2.24a) indicates that the free surface elevation (η) and the velocity (u) are in phase, which is a characteristic of the gravity progressive wave. As for the hypothesis that the velocity is uniform in the transversal section, let's assume that the tidal wave is forcing a vertically homogeneous estuarine channel. In the case that the salinity redistribution is only due to advection, and during the flood the salinity increases gradually towards the mixing zone (MZ). After this flooding event, there will be a salinity decrease due to the influence of the river discharge dammed during the flood. Then, the salinity time variation in a determined longitudinal position (x) will be out of phase by approximately $\pi/2$ or a time interval of 3 h, for a semi-diurnal tidal oscillation in relation to the tidal current as shown in Fig. 2.11.

In this hypothetical estuary, besides the oscillation of the barotropic velocity with the same frequency as the tide, there will also be a low frequency uniform velocity at

Fig. 2.11 Tidal co-oscillation at the mouth of an estuary with infinite length, generating a wave propagation, $\eta = \eta(0, t)$, a tidal current, $u = u(0, t)$ and salinity temporal variation $S = S(t)$ (adapted from Dyer 1973)



the cross section area (A). This component is generated by the river discharge (Q_f), and its intensity (u_f) is given by the ratio Q_f/A . This motion is always oriented seaward ($u_f > 0$), and the resulting velocity in the estuarine channel is:

$$u(x, t) = u_f + U_0 \cos(\kappa x - \omega t + \Phi). \quad (2.25)$$

The tidal excursion (T_E) is defined as the distance travelled by a water particle along the mixing zone, MZ, starting from the rest at the estuarine mouth, during the elapsed time interval between low and high tide. According to this definition, this motion occurs during a time interval of half a tidal period ($T_P/2$). In the assumption that the horizontal axis, Ox , has its origin ($x = 0$) at the estuary mouth, the landward velocity of this volume element is, according to Eq. (2.22), $u(0, t) = U_0 \cos(-\omega t + \Phi)$. To satisfy the initial condition, $u(0, 0) = 0$, it is necessary that, $\Phi = \pi/2$. Then, the tidal excursion, T_E , may be calculated by the mean velocity at the origin during the time interval Δt of half a tidal period ($\Delta t = T_P/2$), times Δt (Harleman 1971) multiplied by the time interval of:

$$T_E = \left[\frac{2}{T_P} \int_0^{T_P/2} u(0, t) dt \right] \frac{T_P}{2} = U_0 \int_0^{T_P/2} \cos(-\omega t + \frac{\pi}{2}) dt = \left(\frac{2U_0}{\pi} \frac{T_P}{2} \right) = \frac{U_0 T_P}{\pi}. \quad (2.26)$$

In Eq. (2.26) the quantity $2U_0/\pi$ is the theoretical mean velocity at the estuary mouth during the time interval of half a tidal period ($T_P/2$). From this equation it is possible to verify that the tidal excursion is proportional to the velocity amplitude (U_0) and the tidal period (T_P); for a semi-diurnal tide $T_P = 43082.0$ s, and, $T_E = 13,713.0U_0$. Then, if the estuary is forced by semidiurnal tides and the amplitude of the tidal velocity is 1.4 m s^{-1} , using Eq. (2.26) the following value for the tidal excursion is calculated: $T_E = 19,200.0 \text{ m}$ ($\approx 19 \text{ km}$). This value is only a first approximation of the tidal excursion and the mixing zone MZ length, because the energy dissipation and the channel geometry have not been taken into account. From the relationship between U_0 and η_0 ($\eta_0 c_0/H_0$), the tidal excursion may be calculated as $T_E = c_0 \eta_0 T_P / \pi H_0$, and is directly proportional to the tidal amplitude η_0 , to the wave celerity and the tidal period T_P , and is inversely proportional to the depth of the estuarine channel, H_0 .

It should be noted that the tidal excursion and the length of saline intrusion are different physical quantities and, for the determination of the second property, extensive theoretical and experimental studies were carried out and presented by Prandle (2009). Its determination in salt wedge and partially mixed estuaries will be studied in Chaps. 9 and 11.

Another quantity associated with the velocity, $u = u(x, t)$ (Eq. 2.22) is the mean root square (u_{rms}). This statistical quantity is equal to the positive value of the root mean square of the mean velocity during one or more complete tidal cycles, that is,

$$u_{\text{rms}} = \sqrt{\frac{1}{T_P} \int_0^{T_P} u^2(x, t) dt} = \sqrt{\frac{1}{2}} U_0 = 0.7 U_0. \quad (2.27)$$

This final has been obtained using trigonometric identities and reducing to the simplest expression.

Let's consider an estuarine channel with finite length L and a tidal wave travelling landward which is reflected at the estuary head, originating a wave in the opposite direction to the original wave. According to the superposition principle, there will be a superposition of these waves. If they have the same frequency, phase velocity and amplitude, and are propagating in opposite directions, with the free surface elevation of the incident and reflected waves denoted by $\eta_1 = \eta_1(x, t)$ and $\eta_2 = \eta_2(x, t)$, respectively, and under the assumption that the phase difference is zero ($\Phi = 0$), it follows the expression for the composite wave:

$$\eta_e(x, t) = \eta_1(x, t) + \eta_2(x, t) = \eta_0[\cos(\kappa x - \omega t) + \cos(\kappa x + \omega t)], \quad (2.28)$$

where ($\eta_e(x, t)$ is the resulting oscillation. By applying the cosine of the addition and subtraction rules to the angles ($\kappa x \pm \omega t$), this equation may be simplified to:

$$\eta_e(x, t) = 2\eta_0 \cos(\kappa x) \cos(\omega t). \quad (2.29)$$

This solution indicates that in a x longitudinal position, the motion of all particles oscillate as a simple harmonic motion. However, the wave amplitude $2\eta_0 \cos(\kappa x)$ varies along the estuary with the following characteristics: it is zero in determined and fixed points and has extreme positive and negative values, resulting in an oscillation of a *stationary wave*. In the above solution (2.29), it is observed that the motion amplitude has the value of zero when $\cos(\kappa x) = 0$, which occurs at the longitudinal points $x = \lambda/4, 3\lambda/4, 5\lambda/4, \dots$, named *nodal* points. In turn, the maximum and minimum values of the amplitude are $2\eta_0$ and $-2\eta_0$, respectively, occurring when $\cos(\kappa x) = \pm 1$, that is, in the points $x = 0, \lambda/2, \lambda, 3\lambda/2, \dots$, named *anti-nodal* points, which are separated by half a wave length ($\lambda/2$). The nodal points are permanently at rest and the wave energy remains steady.

To calculate the longitudinal velocity component of the stationary wave $u_e = u_e(x, t)$, it is necessary to use the continuity Eq. (2.17), resulting the following expression:

$$u_e(x, t) = 2 \frac{\eta_0 \omega}{H_0} \sin(\omega t) \int \cos(\kappa x) dx = 2U_0 \sin(\kappa x) \sin(\omega t), \quad (2.30)$$

which satisfies the boundary condition $u_e(0, t) = 0$. The amplitude of the longitudinal velocity of the water driven by the stationary wave is also dependent of its longitudinal position. When $\sin(\kappa x) = 0$, corresponding to the positions $x = 0, \lambda/2, \lambda, 3\lambda/2, \dots$ (*anti-nodal* points), the velocity is zero. When $\sin(\kappa x) = \pm 1$, that is, in

the nodal points, $x = \lambda/4, 3\lambda/4, 5\lambda/4, \dots$ the amplitude of the velocity is equal to two times those observed in a progressive gravity wave ($2U_0$).

For a fixed longitudinal position (x), Eqs. (2.29) and (2.30) indicate that in the time domain the nodal and anti-nodal points occur at $t = T/4, 3T/4, 5T/4$ and $t = 0, T/2, T, 3T/2 \dots$, respectively, and the free surface oscillation and the velocity are out of phase by a time angle $\pi/2$. By analogy in the case of a progressive wave, considering only the advection of the tidal current in the salinity redistribution of a vertically homogeneous estuary, and under the assumption that the channel length is an integer multiple of $\lambda/2$ ($L = \lambda$, for example), a stationary oscillations will be generated in the mixing zone (MZ). In the anti-nodal times the velocity is zero and the advection in the salinity redistribution is null. However, in the nodal times, flood and ebb tides will occur, driven by wave advection. In a real estuary, the salinity will increase during the flood and decrease during the ebb, due to the fresh water discharge mixing with the coastal saline waters, and the higher salinity values are out of phase in the stationary wave of a $\pi/2$ (Fig. 2.12).

Estuaries don't have a uniform geometry, and in general they become more narrow and shallow towards the estuary head. As such, the tidal amplitude has a

Fig. 2.12 Tidal co-oscillation at the mouth of an estuarine channel with finite length generating a stationary wave $\eta_c(0, t)$, forced by the tidal current $u_c(0, t)$ and salinity $S(t)$ local variations (adapted from Dyer 1973)

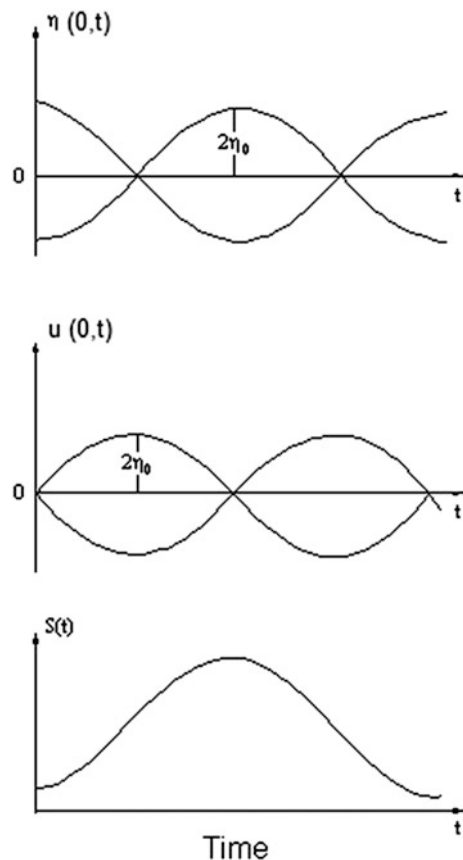
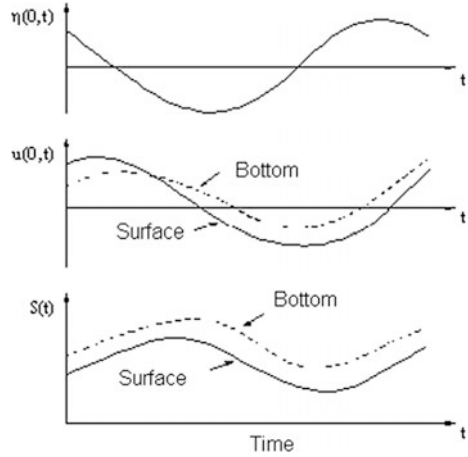


Fig. 2.13 Complex oscillations due to the composition of progressive and stationary waves at the estuary mouth $\eta(0, t)$, due to the tidal $u(0, t)$ and salinity $S(0, t)$ possible scenarios (adapted from Dyer 1973)



tendency to increase up-estuary, but may simultaneously decrease due to the energy dissipation resulting from friction drag, which has been neglected in the theoretical development. As the estuary head usually isn't a close extremity and there will also be energy dissipation in the reflected wave, in most estuaries the wave oscillation is a complex composition of progressive and stationary waves. According to the relative importance of these interacting waves the resulting surface oscillation, the tidal currents and the salinity vary from one estuary to another. A possible scenario is presented in Fig. 2.13.

Applying Eq. (2.27), which defines the root mean square velocity (u_{rms}) to the velocity of the stationary wave (Eq. 2.30), results in:

$$u_{rms} = \sqrt{\frac{1}{T} \int_0^T u_e^2(x, t) dt} = \sqrt{2U_0} \sin(\kappa x) = 1.4U_0 \sin(\kappa x). \quad (2.31)$$

Then, the root mean square of a stationary wave depends on the longitudinal distance (x). As $\kappa = 2\pi/\lambda$, it follows that the $u_{rms} = 0$ or $u_{rms} = 1.4U_0$ at the nodal and anti-nodal points, respectively.

If a non-linear friction drag or a simple linear dependence with a friction coefficient is introduced into the equation of motion (2.14), the solutions for the wave amplitude $\eta = \eta(x, t)$ and the velocity $u = u(x, t)$ will, respectively, show exponential decline and be out of phase with the longitudinal distance (x). Classical solutions may be found in Defant (1960) and, more recently, in the article of Melo and Jorden (1999); in the latter development the channel declivity was also take into account.

2.6 Non-dimensional Numbers

The English physicist and engineer Osborne Reynolds, was able to demonstrate in a classical paper published in 1883, based in laboratory experiments of fluid flow in pipes, that the transition of a laminar (well behaved) motion to a turbulent motion may be determined by the multiplying the product of its mean velocity U by the pipe diameter (D_i), and then dividing by the coefficient of viscosity ν_c , [ν_c] = [L^2T^{-1}]. Then, this dimensionless number is calculated by the ratio UD_i/ν_c , and now is known as the *Reynolds number*; physically, this number compares the relative importance of inertial and viscous forces to determine the characteristics of the flow.

Further investigations of fluid flow in channels with free surface, demonstrated that the pipe diameter may be substituted by the channel depth (H_0) to forecast the regime of motion of liquids with uniform density; the *Reynolds number* is thus defined as:

$$Re = \frac{UH_0}{\nu_c}. \quad (2.32)$$

In general, when $Re < 2.0 \times 10^3$, the flow regime is laminar; however, when Re is of the order of 1.0×10^5 or higher, the motion is fully turbulent, and in a non-homogeneous fluid the mixing is intensified; between the orders of magnitude 2.0×10^3 and 1.0×10^5 the fluid flow regime is transitional.

In estuaries, the mixing of the fresh and salt water is also dependent on the vertical stability of the layers in motion. In experimental investigations (Sternberg 1968) in which the Reynolds number was calculated for estuaries forced by tides and with different bed roughness characteristics, it was observed that Re varied between 1.5×10^5 and 3.6×10^5 , for turbulent motions and the flow over geometrically simple beds became fully turbulent at lower Re values than for beds of complex roughness. In natural water bodies, such as rivers and estuaries, the $Re = 1.5 \times 10^5$ always indicates a transitional change from laminar to turbulent motion.

There are several mechanisms that produce turbulent motions in an estuary: the bed roughness, the velocity vertical shear, the wind stress on the surface, the surface gravity waves and the internal waves. The intensity of the turbulent motion controls the vertical distribution of the physical, chemical, biological and geological properties of the estuarine water mass.

The competition between the vertical stratification and the mixing forms an important process in estuarine dynamics; if the vertical density (salinity) gradient opposes the exchanges of motion by turbulence, an extra velocity shear is necessary to cause mixing (Dyer 1977).

The analysis of the regime of motion in estuaries may also be investigate by the dimensionless *gradient Richardson number* (Ri), defined by the English Meteorologist Lewis Fry Richardson, in 1920, related to studies to forecast of turbulent motions in the atmosphere. This number compares the stabilizing capacity of the vertical density gradient ($\partial\rho/\partial z$) with the destabilizing capacity produced by

the vertical velocity shear ($\partial u/\partial z$), and is very important for indicating the turbulence occurrence in the fluid flow. Its analytical differential expression is:

$$Ri = -\frac{\frac{\rho}{\rho_0} \frac{\partial \rho}{\partial z}}{(\frac{\partial u}{\partial z})^2} \approx -\frac{\beta \frac{\partial S}{\partial z}}{(\frac{\partial u}{\partial z})^2}, \quad (2.33)$$

where the negative signal depends on the orientation of the vertical axis (Oz); in this expression, it is positively oriented in the direction contrary to the gravity acceleration. In the last term on right-hand-side of this definition, it was used the linear equation of state of seawater, $[\rho(S) = \rho_0(1 + \beta S)]$, see Chap. 4], and the simplifications $\rho/\rho_0 = 1$, and $\beta = \text{const.}$ ($\approx 7.0 \times 10^{-4}$ is the approximate value for *salinity contraction coefficient*). This number also provides the quantitative information on the relationship between the buoyancy stabilizing force of the vertical density (salinity) gradient $\partial \rho/\partial z$ ($\partial S/\partial z$), to the destabilizing capacity produced by the vertical velocity shear $\partial u/\partial z$.

The Ri number also indicates the tendency of the water column to be either: very stable and stratified, or weak stratified, indicating the possibility of a turbulent fluid flow. From Eq. (2.33), it follows that $Ri > 0$ correspond to a vertical stability ($\partial \rho/\partial z < 0$ or $\partial S/\partial z < 0$), or alternatively for $Ri < 0$ vertical instability ($\partial \rho/\partial z > 0$ or $\partial S/\partial z > 0$). It should be pointed out that usually the estuarine water mass is in a non-steady-state and the Richardson number is also time dependent $Ri = Ri(x, y, z, t)$.

When the vertical salinity gradient in a given depth is negative ($\partial S/\partial z < 0$), the turbulent flow may be attenuated and the flow regime may develop into a laminar flow. However, above and below this depth the flow regime may be turbulent. Several scientific theoretical and experimental investigations were conducted to understand the mechanisms of the formation and increases of instabilities in stratified fluid interfaces. From these studies it has been found that in uniform motions the transition of the laminar to the turbulent regimes usually occurs for $Ri = 0.25$. When $Ri < 0.25$, the turbulence surpasses the vertical density stratification generating vertical mixing.

The vertical salinity (density) stratification and the velocity shear during a tidal cycle generate variations in the Richardson number at different positions.

For instance, in a given position in the MZ, due to these variations Ri is usually named the local *Richardson number*. An analysis on the variation of this number was made by Blumberg (1975), with hourly measurements of velocity and salinity in the Potomac River (Virginia, USA), during tidal cycles in a water column of 10 m depth. From this analysis, the Ri values were found to vary almost randomly with depth and time, with the maximum positive value occurring at the depth of the maximum vertical salinity gradient. The vertical distribution of Ri presented high vertical stability in some depths, separated by layers of low stability. However, using time mean values of salinity and velocity during the tidal cycle, the highest Ri values occurred at 6 m depth, associated with the highest vertical salinity gradients.

The Richardson number was also applied in studies of the internal structure of the Frazer river estuary (Vancouver, Canada), during length variations of the saline intrusion forced by the tidal oscillations (Geyer and Farmer 1989). The analysis of the calculated values at 0.5 m depth intervals were compared to the vertical profiles of the longitudinal velocity component and the salinity. In the obtained results the Ri value remained very close to 0.25 in the layers above and below the halocline. This number presented high values ($Ri > 25.0$) in the halocline layer with the maximum density vertical gradient and small velocity shear.

Although the variables needed to calculate the Ri number may be accurately measured with the equipment now available to perform profiling of physical properties, it is also useful to use global properties of the water column, and the *layer Richardson number* (Ri_L) has been defined as:

$$Ri_L(t) = \frac{gh(t)\Delta h_v}{\rho \bar{u}^2} \approx \frac{gh(t)\Delta h_v}{\bar{u}^2}, \quad (2.34)$$

where $h = h(t)$ is the local depth, $\Delta \rho_v$ (ΔS_v) is the difference between the bottom density (salinity) and its value at the surface, and $\bar{u} = \bar{u}(t)$ is the mean u -velocity component in the water column which also varies during the tidal cycle Bowden (1978). The time dependence of this dimensionless number was investigated by Dyer and New (1986), showing that; (i) $Ri_L = 20$ is the upper limit for which turbulent mixing occurs near the halocline in partially mixed estuaries; (ii) below this critical number, $Ri_L < 20$, the bottom turbulence becomes effective to the vertical mixing process in the water column; (iii) below $Ri_L = 2$, turbulent mixing is completely isotropic and the water column is unstable; and (iv) for $Ri_L > 20$, the water column is stable with low vertical mixing.

The criteria of Dyer and New (op.cit.) were applied by Miranda et al. (2012) in the analysis of hourly current and hydrographic properties measurements during spring and neap tide in the Piaçaguera estuarine channel, located in the upper reaches of the Santos-São Vicente estuary (Chap. 1, Fig. 1.5). The sampling was made in the austral winter, when the channel was partially mixed and weakly stratified. In the spring tidal cycle (Fig. 2.14a), the calculated values were lower than the critical value, i.e. $Ri_L < 20$ with one exception and it is expected that bottom turbulent mixing became effective, making easier the interchange of the water mass of the bottom and upper layers. During the neap tidal cycle, with a few exceptions, the Ri_L is higher than 20 ($Ri_L > 20$), as shown in Fig. 2.14b, indicating a stable vertical water column, preventing the water masses vertical interchange.

The river discharge may be thought of as a source of deficit of potential energy due to the seawater dilution in the MZ, and, due to the density increase, and the tide as source of kinetic energy to overcome the deficit. Otherwise, the river discharge may be interpreted as a buoyancy source which may be quantified by the product, $g\Delta\rho_H Q_F$, $[g\Delta\rho_H Q_F] = [MLT^{-3}]$, where $\Delta\rho_H$ is the density difference between seawater and freshwater, and is proportional to the barotropic velocity. These physical arguments, associated with laboratory experimental results of circulation in open

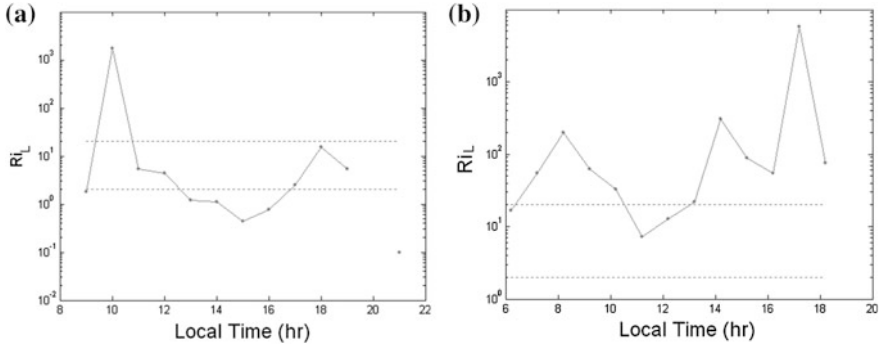


Fig. 2.14 Hourly variation of the layer Richardson number in the Piaçaguera estuarine channel (São Paulo State, Brazil) during spring (a) and neap (b) tidal measurements (according to Miranda et al. 2012)

channels, were used by Fischer (1972) to define a dimensionless number (Ri_e) named *Richardson estuarine*:

$$Ri_e = \frac{g \frac{\Delta \rho_H}{\bar{\rho}} Q_f}{Bu_{rms}^3}. \quad (2.35)$$

In this equation, B is the mean (or local) estuary width, $\bar{\rho}$ is the mean density of the estuarine water mass, and u_{rms}^3 is the third power of the root mean square of the u -velocity component. When the tidal wave is approximate to a progressive wave, we have already shown that $u_{rms} = 0.7U_0$ (Eq. 2.27, Chap. 2). As the horizontal stratification of the estuarine water mass is associated with the low frequency variation of the river, mean density values during tidal cycles must be used to calculate this dimensionless number. This estuarine number is physically interpreted as: when Ri_e is relatively large, the estuary is highly stratified and dominated by the river discharge. Alternatively, if Ri_e has a low value, the estuary is weakly stratified and forced by the tide. In a first approximation, the transitional regime occurs when $0.08 < Ri_e < 0.8$ (Fischer et al. 1979).

To forecast the regime of the flow in highly stratified estuaries an alternative dimensionless number was defined by the comparison of the relative velocity on the upper layer, u_1 , with the velocity of the progressive internal wave propagating in the interface of a highly stratified halocline. Considering a shallow upper layer with depth, H_1 , and density, ρ_1 , in motion with velocity u_1 , over a deep layer with density, ρ_2 ($\rho_2 > \rho_1$), the internal wave celerity (c_0) at the interface, is given by (Defant 1960):

$$c_0 = \sqrt{H_1 g \frac{\Delta \rho}{\rho_2}} = \sqrt{H_1 g'}. \quad (2.36)$$

In this definition $\Delta\rho$ is the density difference of the lower and upper layers ($\rho_2 - \rho_1$) and $g\Delta\rho/\rho_2$ is the *reduced gravity* (g'). An alternative number, which has been called *interfacial Froude number*¹ (Fi), was defined based on a simple theory and experimental results (Stommel and Farmer 1952):

$$Fi = \frac{u_1^2}{H_1 g \frac{\Delta\rho}{\rho_2}} = \frac{u_1^2}{c_0^2}, \quad (2.37)$$

where u_1 is the mean velocity in the upper layer. Thus, the interfacial Froude number compares the fluid speed to the wave speed propagation at the fluid interface. According to the Dyer (1997) in *subcritical* condition $Fi < 1$ the fluid speed is lower than the internal wave celerity. However, when u_1 approaches the internal wave celerity, a wave or perturbation can only travel upstream very slowly and, as the wave energy accumulates, the wave amplitude grows until critical conditions for $Fi = 1$, and the wave will break with energetic mixing. The thickness of the flowing layer will abruptly increase generating an increase in fluid velocity, and the flow changes to a supercritical condition $Fi > 1$. This situation is known as the *internal hydraulic jump*, in analogy to the *hydraulic jump* phenomenon generated when a stratified fluid passes over an obstacle located at the bottom.

The interfacial Froude number may be written as a function of the river discharge and geometric dimensions of the estuary, such as the width (B) and depth, H_0 . Writing the river discharge as $Q_f = u_f B H_0$, the *densimetric Froude number* may be defined as (Hansen and Rattray 1966):

$$F_m = \frac{u_f}{\sqrt{H_1 g \frac{\Delta\rho}{\rho_2}}} = \frac{Q_f}{B H_0 \sqrt{H_1 g \frac{\Delta\rho}{\rho_2}}} = \frac{Q_f}{B H_0 \sqrt{g' H_1}}. \quad (2.38)$$

This number is also known as the *estuarine or internal Froude number*, and a critical number can be achieved by a constriction at the mouth or by a shallow sill depth (Dyer 1997). When the river discharge is weak, $F_m \rightarrow 0$, and the phenomenon of *over-mixing* can occur, and may be observed when the fluid interface (H_1), between the upper and lower layers, is equal to half of the water depth ($1/2 H_0$). This phenomenon has been investigated in laboratory experiments and theoretically by Stommel and Farmer (1952), to explain why, for a stratified estuary, its mouth is a limiting condition to the exchange of salt with the continental shelf.

Equation (2.38) is equivalent to another dimensionless number obtained by the ratio, $u_f/(g H_0 \rho^{-1} \Delta\rho)^{1/2}$, named *densimetric Froude number*, which is the ratio the velocity generated by the river discharge (u_f) divided by the internal circulation

¹The designation of the Froude number was given in honor of William Froude (1810–1879), engineer and naval architect who established the main similarity of reduced ship models and the natural dimensions, introducing the dimensionless number $V/(gL)^{1/2}$ where V and L are the velocity and the ship length at the water level, respectively, and g is the gravity acceleration.

potentially generated by the density gradient $(gH_0\rho^{-1}\Delta\rho)^{1/2}$ (*densimetric velocity*), thus defining the *densimetric Froude number*. This dimensionless number may be applied to estuaries that are highly stratified, where the velocity above the halocline is mainly driven by the river discharge. There is also the *internal Froude number* (Fi), expressed by:

$$Fi = \frac{u}{\sqrt{hg \frac{\Delta\rho}{\rho_2}}} = \frac{u}{\sqrt{hg'}}, \quad (2.39)$$

where the velocity u is a mean velocity value and h is the water layer depth.

The *estuary number* (N_e) was defined by Dyer (1997) by the following ratio,

$$N_e = \frac{T_{PR}F_m^2}{T_P Q_f} = \frac{T_P F_m^2}{R}. \quad (2.40)$$

where T_{PR} is the tidal prism, F_m is the densimetric Froude number (Eq. 2.38), and T_P is the tidal period and Q_f is the river discharge. This definition involves the ratio of the tidal prism to the fresh water volume discharged during a tidal cycle $R = TQ_f$, and some experiments indicate that when $N_e > 0.1$ or $N_e < 0.1$, the estuary is well-mixed or stratified, respectively.

When the wind stress on the surface layer is an important driving force its influence in a highly stratified estuary may be estimated by a dimensionless number named *Wedderburn*. It has been used to investigate the influence of the wind stress in lakes and reservoirs with high vertical temperature stratification. This number, defined by Thompson and Imberger (1980), is calculate by the ratio of the Richardson number and the estuary aspect ratio δ :

$$W = \frac{Ri}{\delta}, \quad (2.41)$$

where, $\delta = L/H_0$, is the ratio of the longitudinal dimension of the water body, L , to its depth H_0 .

Considering an estuary that is vertically stratified and forced predominantly by the wind, the numerator of Eq. (2.41) may be substituted by the following modified Richardson number:

$$Ri = \frac{g\Delta\rho_H H_1}{\rho u_1^2}, \quad (2.42)$$

In this definition $\Delta\rho_H$, u_1 and H_1 are the density variation along the estuary, the velocity, and the depth of the layer over the halocline, respectively. Combining

Eqs. (2.41) and (2.42), it follows the analytical expression of the *estuarine Wedderburn number*, W_e :

$$W_e = \frac{g\Delta\rho_H H_1^2}{\rho u_1^2 L} \approx \frac{g\Delta\rho_H H_1^2}{\tau_w L}, \quad (2.43)$$

in the last expression the quantity ρu_1^2 was approximated by the wind stress shear, τ_w .

Equation (2.43) indicates that W_e is directly proportional to H_1^2 , the horizontal density stratification, and is inversely proportional to the wind stress multiplied by the estuary length. When the wind stress forcing is predominant, $W_e < 1$, and it has the main contribution to the dynamic behavior and mixing of the layer above the halocline. Alternatively, when $W_e \geq 1$ the longitudinal density stratification and the buoyancy due to river input prevails over mixing.

An example on the use of the Wedderburn number to establish the importance of wind stress on the dynamics of two small and shallow (mid-channel depth 1–2 m) estuaries, the Childs and Quashnet, located in the Waquoit Bay (Cape Cod, USA) is presented in the article of Geyer (1997). This study demonstrated the strong influence of wind forcing on salinity structure and flushing characteristics of these estuaries. For most of the observations $W_e < 1$, indicating the important role of wind stress in these estuaries. The sensitive dependence of this number on depth explained why the gentle winds observed during the surveys had such a profound influence on the estuarine dynamics; onshore winds inhibit the estuarine circulation, increasing the longitudinal estuary salinity gradient, and reducing the flushing rate. However, offshore winds enhanced the surface outflow, flushed out the freshwater and reduced the longitudinal salinity gradient.

An alternative expression to the dimensionless flux rate, F_R , may be obtained with theoretical results previously defined in this chapter. This number is determined by the ratio of the volume of river water discharged during a tidal cycle, R , and the tidal prism, T_{PR} . If, A , is the mean transversal section of the estuary mouth, the fresh water volume may be calculated by the product $R = Q_f T = A u_f T$. Thus, under the assumption of a progressive tidal wave propagating landward, $T_{PR} = A (2U_0/\pi)$ and $2U_0/\pi$, are the tidal prism and mean velocity during half tidal cycle, respectively. Then, an alternative expression for the flux ratio is:

$$F_R = \pi \frac{u_f}{U_0} = 3.14 \frac{u_f}{U_0}, \quad (2.44)$$

which is directly and inversely proportional to the velocity of the river discharge and the amplitude of the velocity generated by the tide, respectively. As such, this number will be large or small or when the estuary is dominated by the river discharge or the tide, respectively.

Others dimensionless numbers will be defined in the following chapters related to the estuary classification, according to the acting processes: river discharge, salinity stratification, and mixing processes. Among these there are the

dimensionless numbers: (i) Ekman number, $Ek = \nu_k / f_C D^2$, where ν_k , f_C and D are the kinematic viscosity coefficient, the Coriolis parameter and the vertical length scale, respectively; and; (ii) Kelvin number, $Ke = B / R_D$, where B is the estuary width and R_D is the deformation radius, $R_D = (N_{BV}) / f_C$, with N_{BV} indicating the Brunt-Väisälä frequency which arises in the presence of a background stratification, and the fluid parcel perturbed vertically from its starting position experiences a vertical acceleration.

2.7 Mixing and Entrainment

The term mixing is applied to multitude of physical processes occurring internally in the seawater, which tend to produce uniformities in concentrations of physical, chemical, biological and geological properties. There are two processes that contribute to mixing: (a) *advection* (or advective), characterized by regular patterns of water movement on a macroscopic scale; and (b) diffusion (or diffusive), characterized by microscopic or small-scale irregular movements called turbulence, which together with molecular diffusion give rise to the local exchange of property, without any net transport of water (Okubo 1970; Bowden 1975, 1977). The advective and diffusive tidal forcing are the main processes which produces to the mixing of the river and salt water, contributing to the salinity stratification characteristics.

The mixing of salt and fresh water is carried out by a combination of turbulence generated by the current shear mainly due to tidal currents in the water column, and at the sea bed. These two effects vary in their magnitudes and timing during the tide, as well as in different estuarine types, as the salinity stratification and tidal velocities changes. Competition between stratification and mixing play a crucial part in estuarine dynamics because when the fluid is stratified, the density gradient resists to the exchanges of momentum by the turbulence and an extra velocity shear is necessary to cause mixing, and thus influence the distribution of natural water properties and those discharged into the estuaries. The role of internal mixing processes (mixing, turbulent diffusion and internal waves) and its main characteristics are presented in the Dyer's (1997) book and a brief outline is given below.

In an estuary with small tidal amplitude that may be neglected and a moderate or high river discharge, the water discharged into the estuary head moves seaward flowing persistently on the surface layer due to its relatively low density. During this flow, and at $Ri > 0.25$, instabilities at the stratified interface take the form of *cusps* or progressive interfacial *Holmboe waves*, which grow in height and became sharper crested. Eventually they break, and wip-like elements of denser water are ejected from the crests into the upper lighter layer. This upward transference of salt water is unidirectional, and this phenomenon is known as *entrainment*. Its importance to the estuarine dynamics has been presented in the pioneering article of Keulegan (1949) based on laboratory experiments. A vivid description of mixing in a natural estuary has been given by Farrel (1970—quoted in Dyer 1997, p. 45), showing that entrainment is a one-way process in which a less turbulent water mass

become drawn into a turbulent layer; it is an internal mechanism, besides the advection and turbulent diffusion to the estuarine mixing, occasioning salinity increase in the upper layer. The balance of the volume transport down and up-estuary in the upper and lower layers, as well as the transport associated with the entrainment, were calculated using the continuity of fresh water by Tully (1958).

The above process may be superimposed to the turbulent diffusion which may be subdivided into three types (Bowden 1977): (1) On or near the bottom due to the frictional shear, which propagates into the water column; (2) Generated inside the water layer due to the turbulent diffusion, which may be dumped by the vertical stratification; and (3) Turbulent diffusion on the free surface due to the wind stress, generating gravity waves and drift currents. Generally, when the river discharge is intense and the tidal amplitude is small the entrainment is the mechanism which predominates; however, the higher the tidal amplitude, the higher is its influence to generate mixing through the processes of advection and diffusion.

The estuarine flow usually occurs in a transitional regime from laminar to turbulent, generated by microscopic and macroscopic scales of motion, respectively. Mainly due to tidal oscillations the entrainment, turbulent diffusion and advection are the processes responsible for the mixing of the fresh and salty water masses, the local and spatial salinity, and temperature, as well as, the concentrations of natural properties and pollutants launched into the estuaries. Unfortunately the fresh water discharged into estuaries and its geometry has been altered and this external interference will alter the circulation, the assimilation and mixing processes, and water mass renewal in these very important coastal ecosystems.

References

- Andutta, F. P. 2011. O Sistema Estuarino dos Rios Caravelas e Peruípe (BA): Observações, Simulações, Tempo de Residência e Processos de Difusão e Advecção. Tese de Doutorado. São Paulo, Instituto Oceanográfico, Universidade de São Paulo. 121 p.
- Arons, A. B. & Stommel, H. 1951. "A Mixing-Lenght Theory of Tidal Flushing". *Trans. Am. Geophys.Un.*, 32(3):419–421.
- Blumberg, A. F. 1975. A Numerical Investigation into the Dynamics of Estuarine Circulation. Tech. Rept. Chesapeake Bay Institute, The Johns Hopkins University. n. 91. 110 p. + Apêndices.
- Bonetti, J. F. & Miranda, L. B. de. 1997. "Estimativa da Descarga Fluvial no Sistema Estuarino-Lagunar de Cananeia-Iguape". *Rev. Bras. Oceanogr.*, São Paulo, 45(1/2):89–94.
- Bowden, K. F. 1975. Oceanic and Estuarine Mixing Processes. In *Chemical Oceanography*, Academic Press, London, Chapter 1, pp. 1–41.
- Bowden, K. F. 1977. Turbulent Processes in Estuaries. *Estuaries, Geophysics, and the Environment*. National Academy of Sciences, Washington, D. C., pp. 46–56.
- Bowden, K. F. 1978. "Mixing Processes in Estuaries". In: Kjerfve, B. (ed.). *Estuarine Transport Processes*. University of South Carolina Press, Columbia, pp. 11–36. (Belle W Baruch Library in Marine. Science, 7).
- Coleman, J. M. & Wright, L. D. 1971. *Analysis of Major River Systems and Their Deltas: Procedures and Rationale, with two Examples*. Baton Rouge, Louisiana State University Press. 125 p.

- Davies, J. H. 1964. "A Morphogenic Approach of World Shorelines". *Z. Geomorphology*, 8:127–142.
- Defant, A. 1960. *Physical Oceanography*. Oxford, Pergamon Press, vol. 2. 598 p.
- Doodson, A. T. 1928. The Analysis of Tidal Observations. *Phyl. Trans. R. Soc. Lond., Series A*, 227:223–279.
- Dyer, K. R. 1973. *Estuaries: A Physical Introduction*. London, Wiley. 140 p.
- Dyer, K. R. 1977. Lateral Circulation Effects in Estuaries. *Estuaries, Geophysics and the Environment*. Washington, D. C., National Academy of Sciences, pp. 22–29.
- Elliott, A.J. 1978. Observations of the Meteorologically Induced Circulation in the Potomac Estuary. *Estuarine, Coastal Marine Science*, 6, 285–299.
- Farrel, S.C. 1970. Sediment Distribution and Hydrodynamics Saco River and Scarboro Estuaries, Maine. Cont. 6-CRG, Dept. Geol. Univ. Mass. (quoted in Dyer, 1997), p. 45).
- Fischer, H. B. 1972. Mass Transport Mechanisms in Partially Stratified Estuaries. *J. Fluid Mech.*, 53:672–687.
- Fischer, H. B.; List, E. J.; Koh, R. C. Y.; Imberger, J. & Brooks, N. H. 1979. *Mixing in Inland and Coastal Waters*. New York, Academic Press. 483 p.
- Franco, A. S. 1988. *Tides: Fundamentals, Analysis and Prediction*. São Paulo, Fundação Centro Tecnológico de Hidráulica. 249 p.
- Franco, A. S. 2000. MARE'S: Programa para Previsão e Análise. In: *Manual*, BSP, São Paulo. 36 p.
- Franco, A. S. 2009. *Marés – Fundamentos, Análise e Previsão*. Diretoria de Hidrografia e Navegação. Rio de Janeiro, 2nd ed., 344 p.
- French, P. W. 1997. *Coastal and Estuarine Management*. London, Routledge. 251 p. (Environmental Management Series).
- Geyer, W. R. 1997. Influence of Wind on Dynamics and Flushing of Shallow Estuaries. *Estuar. Coast. Shelf Sci.*, 44:713–722.
- Geyer, W. R. & Farmer, D. M. 1989. Tide-Induced Variations of the Dynamics of a Salt Wedge Estuary. *J. Phys. Oceanogr.*, v. 19, pp. 1060–1072.
- Gill, A. E. & Schumann, E. H. 1979. The Generation of Long Shelf Waves by the Wind. *J. Phys. Oceanogr.*, 4:83–90.
- Hansen, D. V. & Rattray Jr., M. 1966. New Dimensions in Estuary Classification. *Limnol. Oceanogr.*, 11(3):319–325.
- Harleman, D. R. F. 1971. One-Dimensional Models. In: Ward Jr., G. H. & Espey Jr., W. H. (eds.). *Estuarine Modelling: An Assessment Capabilities and Limitations for Resource Management and Pollution Control*. Austin, Tracor, pp. 34–89.
- Holland, H. D. 1978. *The Chemistry of the Atmosphere and Oceans*. New York, Wiley. 351 p.
- Ippen, A. T. & Harleman, D. R. F. 1961. One-Dimensional Analysis of Salinity Intrusion in Estuaries. Committee on Tidal Hydraulics. Tech. Bull. Corps of Engineers U. S. Army, n. 5. 120 p.
- Jay, D. A. 2010. Estuarine Variability. In: ed. Valle-Levinson A. *Contemporary Issues in Estuarine Physics*. Cambridge University Press, pp. 62–99.
- Keulegan, G. H. 1949. Interfacial Instability and Mixing in Stratified Flows. *J. Res. U. S. Geol. Surv.*, 43:487–500.
- Kjerfve, B. 1990. *Manual for Investigation of Hydrological Processes in Mangrove Ecosystems*. New Delhi, Unesco/UNDP. 79 p.
- Kjerfve, B. & Ferreira, H. O. 1993. Tidal Bores: First Ever Measurements. *Ciência Cult.*, São Paulo, 45(2):135–137.
- Kjerfve, B.; Schettini, C. A. F.; Knoppers, B.; Lessa, G. & Ferreira, H. O. 1996. Hydrology and Salt Balance in a Large, Hypersaline Coastal Lagoon: Lagoa de Araruama, Brazil. *Estuar. Coast. Shelf Sci.*, 42:701–725.
- Kjerfve, B.; Ribeiro, C. H. A.; Dias, G. T. M.; Fillippo, A. M. & Quaresma, V. S. 1997. Oceanographic Characteristics of an Impacted Coastal Bay: Baía de Guanabara, Rio de Janeiro, Brazil. *Continental Shelf Res.*, 17(13):1609–1643.

- Kosoun, V.I.; Sokolov, A.A.; Budyko, M.I.; Voskresensky, K.P.; Kalinin, G.P.; Konoplyantsev, A.A.; Korotkevich, E.S.; Kuzin, P.S. & Lvovitch, M.I. 1974. World Water Balance and Water Resources of the Earth, prepared by the U.S.S.R. National Committee for the International Hydrological Decade, V.I. Kosoun, Editor-in-Chief, Leningrad.
- Kvale, E.P. 2006. The origin of neap-spring tidal cycles. *Marine Geology*, 235, pp. 5–18.
- Lacerda, L.D., Kjerfve, B., Salomons, W. and Kremer, H.H. 2002. Regional assessment and synthesis: South America. In (Eds. Lacerda, L.D.; Kremer, H.H.; Kjerfve, B.; Salomons, W.; Marshall Crossland J.I.
- Leblond, P.H. 1979. Forced Fortnightly Tides in Shallow Rivers. *Atmosphere. Ocean*. 17(3):253–264.
- Leblond, P.H. & Mysak, L.A. 1978. *Waves in the Ocean*. Elsevier. Amsterdam, 602 p.
- Miranda, L. B.; Castro, B. M. de. & Kjerfve, B. 1998. Circulation and Mixing in the Bertioga Channel (SP, Brazil) Due to Tidal Forcing. *Estuaries*, 21(2):204–214.
- Miranda, L. B.; Dalle Olle, E.; Bérghamo, A.L.; Silva, L.S. & Andutta, F.P. 2012. Circulation and salt intrusion in the Piaçaguera Channel, Santos (SP). *Braz. J. Oceanography*, 60(1):11–23.
- Medeiros, C. & Kjerfve, B. 1993. Hydrology of a Tropical Estuarine System: Itamaracá, Brazil. *Estuar. Coast. Shelf Sci.*, 36:495–515.
- Mello, E. 1998. Considerações sobre a Hidráulica de Canais Fluviais e Canais de Maré. *Rev. Bras. Rec. Hid.* 3(2):95–107.
- Melo, E. & Jorden, V. 1999. Tide Penetration in Coastal Waters. *Proceedings of the Fifth International Conference on Coastal and Port Engineering in Developing Countries*. Cape Town, South Africa, pp. 1771–1781.
- Nichols, M. M. & Biggs, R. B. 1985. Estuaries. In: Davis R. A. (ed.). *Coastal Sedimentary Environments*. Berlin, Springer-Verlag, pp. 77–186.
- Okubo, A. 1970. Oceanic Mixing. The Johns Hopkins University. Chesapeake Bay Institute. Tech. Rept., n. 62. 140 p.
- Pawlowicz, R.; Beardsley, B. & Lentz, S. 2002. Classical tidal harmonic analysis including error estimates in MATLAB® using T-TIDE. *Computers & Geosciences*, v. 28:939–937.
- Pedloski, J. 1979. *Geophysical Fluid Dynamics*. 2. ed., New York, Springer-Verlag. 624 p.
- Pritchard, D. 2009. *Estuaries: Dynamics, Mixing, Sedimentation and Morphology*. Cambridge University Press, N.Y., 236 p.
- Pritchard, D. W. 1952. Salinity Distribution and Circulation in the Chesapeake Bay Estuarine System. *J. Mar. Res.*, 11(1):106–123.
- Pritchard, D. W. 1955. Estuarine Circulation Patterns. *Proc. Am. Soc. Civ. Eng.*, 81:717–11.
- Pritchard, D. W. 1958. The Equations of Mass Continuity and Salt Continuity in Estuaries. *J. Mar. Res.*, 17:412–423.
- Platt, T.; Mann, K.H. & Ulanowicz, R.E. (Eds.) 1981. *Mathematical Models in Biological Oceanography*. The Unesco Press, 156 p.
- Schettini, C. A. F. 1994. Determinantes Hidrológicos na Manutenção da Condição Hipersalina da Lagoa de Saquarema. Dissertação de Mestrado, Niterói, Universidade Federal Fluminense. 75 p.
- Schettini, C. A. F. 2002. Caracterização Física do Estuário do Rio Itajaí-açu, SC. *Revista Brasileira Recursos Hídricos*, 7(1):123–142.
- Sternberg, R. W. 1968. Friction Factors in Tidal Channels with Differing Bed Roughness. *J. Mar. Geol.*, 6:243–260.
- Stommel, H. & Farmer, H. G. 1952. Abrupt Change in Width in Two-layer Open Channel Flow. *J. Mar. Res.*, 11:203–214.
- Thompson, R. O. R. Y. & Imberger, J. 1980. Response of a Numerical Model of a Stratified Lake to Wind Stress. *Proc. 2nd Intl Symp. Stratified Flows*, Trondheim, pp. 562–570.
- Tully, J. P. 1958. On Structure, Entrainment and Transport in Estuarine Embayments. *J. Mar. Res.*, 17:523–535.
- von Arx, W. S. 1962. *An Introduction to Physical Oceanography*. Addison-Wesley, Massachusetts. 422 p.

Quoted References

- Defant, A. 1961. *Physical Oceanography*. Oxford, Pergamon Press, vol. 1. 729 p.
- Dyer, K. R. 1997. *Estuaries: A Physical Introduction*. 2. ed., Chichester, Wiley. 195 p.
- Geyer, W.R. 2010. Estuarine salinity structure and circulation. In: ed. Valle-Levinson A. *Contemporary Issues in Estuarine Physics*. Cambridge University Press, pp. 12–26.

Fundamentals of Estuarine Physical Oceanography

Bruner de Miranda, L.; Andutta, F.P.; Kjerfve, B.; Castro

Filho, B.M. de

2017, XXXII, 480 p. 138 illus., 17 illus. in color.,

Hardcover

ISBN: 978-981-10-3040-6